Győre, D., Pujol, M., Gilfillan, S. M.V. and Stuart, F. M. (2021) Noble gases constrain the origin, age and fate of CO2 in the Vaca Muerta Shale in the Neuquén Basin (Argentina). *Chemical Geology*, 577, 120294. (doi: 10.1016/j.chemgeo.2021.120294)

There may be differences between this version and the published version. You are advised to consult the published version if you wish to cite from it.

http://eprints.gla.ac.uk/240249/

Deposited on 27 April 2021

Enlighten – Research publications by members of the University of Glasgow
http://eprints.gla.ac.uk

Noble gases constrain the origin, age and fate of CO_2 in the Vaca Muerta Shale in the Neuquén Basin (Argentina)

Domokos Györe[a]*, Magali Pujol[b], Stuart M.V. Gilfillan[c] and Finlay M. Stuart[a]

[a] Isotope Geosciences Unit, Scottish Universities Environmental Research Centre (SUERC), East Kilbride G75 0QF, UK
[b] TOTAL EP, CSTJF, Avenue Larribau, 64000 Pau, France
[c] School of GeoSciences, University of Edinburgh, Edinburgh EH9 3FE, UK

*Author for correspondence:

E-mail: gyoredomokos@gmail.com

Keywords

Subsalt CO_2, isotope tracing, mass spectrometry, stable isotope, noble gas isotope, unconventional, shale gas

Highlights

- Elevated CO_2 levels are consistently encountered when deep-rooted faults overlap with shallower faults in the basin.
- Noble gases highlight a magmatic origin for CO_2 encountered in the Vaca Muerta Shale.
- Noble gas isotopes trace source and evolution of gas composition in the Vaca Muerta Shale.

TOTAL Classification: Restricted Distribution
TOTAL - All rights reserved

Abstract

Unconventional hydrocarbon resources such as shale oil/gas and coal-bed methane have become an increasingly important source of energy over the past decade. The Vaca Muerta Shale (Neuquén Basin, Argentina) contains the second largest technically recoverable quantity of shale gas in the world. Exploitation of the play has been complicated by elevated concentrations of CO_2 in several fields, the origin of which is currently poorly understood. Elevated CO_2 levels are consistently encountered when deep-rooted faults in the Auquilco Evaporite Formation, present below the Vaca Muerta Shale, overlap with shallower faults that propagate from the top of evaporites into the shale, indicating a sub-evaporate origin of the CO_2. Here we report new isotopic analysis of CO_2-rich gases from two producing fields. CO_2 concentrations increase with $C_1/(C_2+C_3)$ values (4.8 – 33.5) and fractionation of $\delta^{13}C_{CO2}$ (-0.9 to -7.7 ‰), suggest that CH_4 have been displaced by CO_2 which entered the shale after hydrocarbon maturation. The noble gas composition ($^3He/^4He$ of 3.43 – 3.95 R_A, where R_A is the atmospheric ratio of 1.399 x 10^{-6}, $^{21}Ne/^{22}Ne$ of 0.0310 - 0.0455, $^{20}Ne/^{22}Ne$ of 9.89 - 10.52, $^{40}Ar/^{36}Ar$ of 2,432 – 3,674 and $CO_2/^3He$ 6.8 - 20.2 x 10^7) of the gases is consistent with mixing of magmatic CO_2 with crustal hydrocarbon-rich gases and provides evidence for the loss of significant CO_2. Using inverse modelling techniques, we determine that the magmatic gas has a $^3He/^4He$ of 3.95 - 4.08 R_A, $CO_2/^3He$ of 8.8 - 16 x 10^8 and $^{20}Ne/^{22}Ne$ of $12.13^{+0.08}_{-0.10}$, $^{21}Ne/^{22}Ne$ of $0.074^{+0.004}_{-0.003}$. Based on the radiogenic He and Ne this is consistent with a depleted asthenosphere mantle source, which has been trapped in the crust since 6.0 – 22.8 Ma. This is significantly younger than Late Cretaceous maturation of the hydrocarbon source rocks. Mantle melting as a result of asthenosphere upwelling induced by the collision of the South Chile Ridge and the Chile Trench at ~14 Ma is the most likely source of the CO_2. Gases from below the shale contain two air saturated water-derived noble gas components, distinguished on the basis of $^{20}Ne^{\dagger}/^{36}Ar$, $^{84}Kr/^{36}Ar$, $^{132}Xe/^{36}Ar$ ratios. These are consistent with early and late stage open system Rayleigh fractionation of groundwater-derived noble gases. We find evidence that these mix with the magmatic component prior to entering the Vaca Muerta and mixing with an adsorption derived gas retained in the source kerogen.

TOTAL Classification: Restricted Distribution
TOTAL - All rights reserved

1. Introduction

Unconventional hydrocarbon production, including shale gas and oil, tight gas and coal-bed methane, has emerged as a significant energy source in the 21st Century. It has been driven by the development of horizontal drilling techniques and high-volume hydraulic fracturing technologies. Global production of unconventional hydrocarbons has significantly increased over the past decade, predicted to make up ~20% of the global natural gas market in 2020, rising to ~45% by 2040 (IEA, 2019). Argentina has the second largest technically recoverable unconventional hydrocarbon resources in the world, with the majority of this being hosted within the Vaca Muerta Formation in the Neuquén Basin (Dominguez et al., 2016). The potential exploitation of this resource is assisted by Argentina's experience and existing infrastructure from decades of conventional hydrocarbon extraction in the Neuquén Basin, along with the social acceptance of the industry in the area. Unconventional hydrocarbon pilot projects have been developed in the region since 2009, with fifteen currently in active operation (Gomes and Brandt, 2016).

A major restriction in upscaling gas extraction to commercial levels in many fields is the potential risk posed by the presence of large quantities of uneconomic CO_2 throughout the Neuquén Basin. A clear understanding of the origin of the CO_2 and how it has been introduced into the reservoir lithologies is essential in order to reduce the risks for the development plan in the region. Currently, there is no consensus as to the source of this CO_2. CO_2 in the basin may have a deep magmatic origin based on limited stable isotope and noble gas analysis (Prinzhofer et al., 2009; Brisson et al., 2020). A more recent isotope study of CO_2 from the Vaca Muerta Shale implies an organic origin (Ostera et al., 2016).

Noble gases (He, Ne, Ar, Kr and Xe) are present in natural fluids in trace quantities and provide a complementary tracing tool along with major gas concentrations and stable isotopes. Noble gas analysis of produced fluids for subsurface reservoirs has been used to determine the origin of hydrocarbons and CO_2, their migration and interaction with reservoir fluids in natural gas fields (e.g. Ballentine and O'Nions, 1994; Ballentine and Sherwood Lollar, 2002; Gilfillan et al., 2008; 2009; 2014; Hunt et al., 2012; Karolytė et al., 2019; Pinti and Marty, 1995), CO_2-fluid interaction in enhanced oil recovery and carbon storage test sites (Györe et al., 2017; 2015; Nimz and Hudson, 2005; Stalker et al., 2015) and hydrocarbon accumulations from coal-bed methane fields (Chen et al., 2019; Györe et al., 2018; Moore et al., 2018; Zhou et al., 2005). In shales, the heavy noble gases (Kr, Xe) can be used to track fluid origin due to their high adsorption potential on organic matter (Hiyagon and Kennedy,

TOTAL Classification: Restricted Distribution
TOTAL - All rights reserved

1992; Kennedy et al., 2002; Podosek et al., 1980; Torgersen and Kennedy, 1999). Kr and Xe have recently been used to trace the origin and interaction history of hydrocarbons in shales (Byrne et al., 2020; Darrah et al., 2015; 2014; Heilweil et al., 2015; Wen et al., 2015; 2016; 2017).

Here we use $\delta^{13}C_{CO2}$ and noble gases to trace the origin of CO_2 in produced gas from two conventional and unconventional hydrocarbon fields in the Vaca Muerta Shale and the overlying Mulichinco Formation in the southern part of the Neuquén Basin. Through the integration of seismic profiles from the basin with the non-radiogenic noble gas data, we constrain the history of fluid interaction that controls the variable CO_2 and hydrocarbon concentrations in the study sites.

2. Study site

2.1. Geological history

The Neuquén Basin is located in west-central Argentina and central Chile (Figure 1A), covering more than 120,000 km^2. The basin extends from 32° to 40°S, from the south of Mendoza province to the extra-Andean region of Neuquén. It is bounded to the west by the Andes, to the south and north-east by the North Patagonian Massif and Sierra Pintada Massif, respectively (Howell et al., 2005). It first formed in the Late Triassic-Early Jurassic as a result of extension during the breakup of Pangea and southwestern Gondwana. Individual grabens that developed during rifting filled with clastic sediments and syn-rift volcanoclastic deposits (Franzese and Spalletti, 2001). Active subduction on the western Gondwana margin generated a back-arc basin that accumulated regressive-transgressive cycles of sedimentation (Vergani et al., 1995).

In the Middle Jurassic to Early Cretaceous, the isolated basins merged, to produce a broad single basin, as a result of the transition to neutral subduction regime and the evolution of a volcanic arc. Basin sedimentation was dominated by thermal subsidence and eustatic sea-level changes, resulting in classic filling sequence of Mesozoic marine and continental rocks such as the marine carbonate La Manga Formation, the fluvial sandstone Tordillo Formation and evaporitic rocks such as the Auquilco Evaporite (Gulisano and Gutiérrez Pleimling, 1995; Palma et al., 2009; Spalletti et al., 2008). Deposition of the Tithonian - Early Valanginian Vaca Muerta Formation, composed of bituminous shales deposited under anoxic conditions of shelf and slope marine settings, occurred during the sag stage. It conformably

TOTAL Classification: Restricted Distribution
TOTAL - All rights reserved

overlies the permeable marine and continental rocks mentioned above. The formation is characterised by a high total organic matter content (TOC) from 3 to 8%, with peak values of 12% and dominant Type II kerogen (Sylwan, 2014).

In the Early Cretaceous the tectonic regime transitionally changed to compression, due to a decrease in the subduction angle and the beginning of the Andean orogeny. This resulted in the inversion of the basin by reactivation of the original extensional structures (Vergani et al., 1995). The associated depositional environments became restricted hypersaline marine with deposition of dolomite, gypsum, halite and sylvinite and of continental fluvial and lacustrine sediments (Spacapan et al., 2018). The block was uplifted in Late Cretaceous–Eocene (Zamora Valcarce et al., 2009) and in two Miocene uplift events between 25 Ma and 14 Ma (Gorring et al., 1997). Magmatism in response to subduction of the Pacific plate is recorded in the intrusion of sub-volcanic dykes and sills at ~9 Ma (Ramos, 1981), the eruption of Pliocene alkali-basalts at ~4.5 Ma and alkali intraplate volcanism at 1.8 Ma (Kay et al., 2004) (Figure 1B).

Two generations of persistent faulting are present within the basin. NNW trending faults are pervasive throughout, rooted at depths of at least 4.4 km into the Upper Jurassic Auquilco Evaporite Formation. They were initially normal faults, generated during the Late Triassic – Early Jurassic rifting, but have subsequently been reactivated as reverse faults during the early to late Cretaceous basin inversion. N70 trending strike-slip faults, rooted from the top of Auquilco Formation evaporites up to the Mulichinco Formation (through the Vaca Muerta) are also widespread in the basin (Gangui and Grausem, 2014) (Figure 2). Initial hydrocarbon exploration of the basin has encountered elevated CO_2 concentrations in regions where the two fault systems intersect. This implies that the CO_2 most probably originates from below the Upper Oxfordian (~160 Ma) Auquilco Evaporite Formation.

2.2. Hydrocarbons in the Neuquén Basin

The Neuquén Basin hydrocarbons have been generated from two organic-rich source rocks contained in the Los Molles and the Vaca Muerta formations. This study focuses on gases encountered in and migrated from the Vaca Muerta Formation. This formation predominantly consists of a Tithonian–Lower Valanginian (Upper Jurassic-Early Cretaceous) basinal marine black shales, shelf marine sandstones, marls and limestones with a bituminous section in its lower part. It is on average ~200 m thick but thickens to ~350 m in the north of the basin. It

TOTAL Classification: Restricted Distribution
TOTAL - All rights reserved

outcrops at the surface in the west of the basin and reaches depths of 2700 m in the east. The oil and gas produced in the formation is believed to have migrated into the overlying Quintuco and Mulichinco Formations 25-14Myr ago (Chebli et al., 2011; Legarreta et al., 1999; Rainoldi et al., 2014). The majority of the hydrocarbons in the Vaca Muerta–Mulichinco system are extracted from the Aguada Pichana, Parva Negra and Sierra Chata fields (Vergani et al., 1995). The Mulichinco Formation is a 200 m thick Valanginian age deposit, consisting of alternating layers of distal shelf black shales, fine-grade calcareous sandstones and limestones. Conventional hydrocarbon production from the Mulichinco Formation started in the early 1990s (Hogg, 1993) and exploration for unconventional oil and gas in the Vaca Muerta commenced in 2008, with the first discovery occurring in 2010. Exploitation of these unconventional resources utilises the existing conventional hydrocarbon infrastructure (Dominguez et al., 2016; Gomes and Brandt, 2016).

3. Sampling and analytical techniques

The sampling for this study targeted two fields and two formations located in the Neuquén Basin. The two fields, named A and B, are separated by 200 km. Field A is located in the southern portion of the basin, and field B is located north of field A. Ten gas samples were collected from field A and two from field B. Eight ‘unconventional’ gases from field A were obtained by the hydraulic fracturing of the Vaca Muerta Shale with the remaining two being ‘conventionally’ produced gases from the Mulichinco Formation. The gases obtained from two wells sampled in field B are also sourced from the hydraulic fracturing of the Vaca Muerta Shale (Table 1). In field A only gas is produced, GOR values are between 19,000 (well #10) and 23,000 (well #9). In field B, light oil is produced, GOR is 408 (well #11) and 490 (well #3).

Samples were collected directly from high pressure well heads or gas separator in April 2016. Well head/gas separator pressures ranged from 1.5 and 5.9 MPa and temperatures varied from 10 to 58°C. Gases were collected from gas separator when possible to minimise water and/or oil content. A regulator was attached to the well head/separator and the outlet split the gas flow into i) an Isotube unit (for major and stable isotopic composition), and ii) an all-metal unit with double cells connected to each other via Swagelok VCR seals (for noble gas composition determination) via 6 mm outer diameter stainless steel pipe. The noble gas unit remained closed when a sample was collected in the Isotube. The Isotube was flushed for 2

TOTAL Classification: Restricted Distribution
TOTAL - All rights reserved

minutes with well gas prior to being sealed with a valve at the downstream end, followed by closing the valve at the upstream end. During noble gas sampling the Isotube unit was sealed from gas flow. Noble gas cells were flushed for 10 to 15 minutes after which the valves of the unit were closed sequentially from the downstream to the upstream end. Pressure in both Isotube and noble gas units was regulated to be 0.3 - 0.4 MPa above atmosphere prior to sealing. The effective hydrocarbon production period since hydraulic fracturing had been undertaken in each well exceeded 6 months in all cases, in order to avoid fractionation of volatile species caused by the stimulation of the shale.

Molecular composition of the gases was determined by gas chromatograph using a thermal conductivity detector technique with the relative standard deviation of 1%. Isotopic ratios were determined by a GC-IRMS. Reported δD_{CH4} values are relative to V-SMOW (Gonfiantini, 1984) and $\delta^{13}C_{CO2,CH4}$ are relative to V-PDB international standard (Coplen, 1994; Craig, 1957) and determined with the error of 0.4‰ (2σ). Noble gas isotope analysis was carried out from a single cylinder of the double-cell unit at SUERC, using a MAP 215-50 static vacuum mass spectrometer following the procedures described previously (Györe et al. 2017; 2015). No significant contribution of $^{20}NeH^+$ at m/z = 21 was found during sample analysis (Györe et al., 2019). Mass spectrometer sensitivity and mass discrimination were determined using the Helium Standard of Japan (HESJ) international standard (Matsuda et al., 2002) for He and air (Eberhardt et al., 1965; Györe et al., 2019; Mark et al., 2011, Ozima and Podosek, 2002) for Ne, Ar, Kr, Xe. We calculate $^3He/^4He$ ratios relative to air (1.399×10^{-6}, Mamyrin et al. (1970)). While we are aware of more recent and more accurate determinations of $^3He/^4He_{air}$ (Mishima et al., 2019 and references therein) we expect further, independent confirmation to establish an updated standard as recommended by Mishima et al. (2019). The ~4% difference in values will have no impact in our conclusions.

4. Results

4.1 Major gases and stable isotopes

Saturated hydrocarbons (C_1, C_2 and C_3) and CO_2 comprise between 97.1% (well #10) and 99.1% (well #12) of the gases. CH_4 concentrations in the Vaca Muerta gases vary between 82.1% (well #10) and 88.4% (well #2) in field A, compatible with the wet to dry gas window and between 75.4% and 79.9% in field B, compatible with the fact that light oil is produced. The Mulichinco Formation gas CH_4 content is between 70.8% and 91.8. $C_1/(C_2+C_3)$ ratios

TOTAL Classification: Restricted Distribution
TOTAL - All rights reserved

vary between 4.8 (well #3 & 11) and 33.5 (well #7). C_4 and C_5 hydrocarbons are less than 0.9 and 0.4% respectively for all samples (Table 1).

The carbon isotopic composition of the CH_4 from field A (from both conventional and unconventional sources) are between -42.1‰ and -37.0‰, while hydrogen isotope composition varies from -166‰ to -156‰. This is consistent with a thermogenic origin for the methane (Figure 3A & B, Table 2) (Snodgrass and Milkov, 2020) in line with the commercially most successful shale plays (Milkov and Etiope, 2018; Milkov et al., 2020). $\delta^{13}C_{CH4}$ and δD_{CH4} from field B are comparable (-39.7‰ to -37.0‰ and -163‰ to -156‰, respectively) but the lower $C_1/(C_2+C_3)$ values, suggest the gas may be less mature than that from field A (Table 1). The $\delta^{13}C_{CH4}$ and molecular compositions overlap values from Vaca Muerta gases determined previously (Brisson et al., 2020; Ostera et al., 2016). The increase of $\delta^{13}C$ of hydrocarbons with increasing mass ($C_2 – C_5$) is consistent with the 'normal' trend of increasing maturity (Milkov et al., 2020) (Figure 3C & 3D, Table 2) and further supports the contention that field B hydrocarbons are less mature.

The CO_2 content of the Vaca Muerta Shale gases varies between 0.4% (well #10) and 9.3% (well #4). In the gases from the Mulichinco Formation CO_2 concentrations range from 0.08% (well #5) to 24.2% (well #6). $\delta^{13}C_{CO2}$ values from the Vaca Muerta from field A are between -0.9‰ and -3.2‰ and are much lighter in the two wells from field B (-7.5 and -7.7‰) (Table 1 & 2). This is indicative of either a magmatic or metamorphic origin for the CO_2 (e.g. Sherwood Lollar et al., 1997). They are significantly heavier than those recorded by Ostera et al. (2016) (-9.6 to -16.7 ‰). The Mulichinco Formation gases have distinct $\delta^{13}C_{CO2}$ (-8.6‰ and -12.8‰). While the origin of CH_4 based on the relationship between $\delta^{13}C_{CO2}$ and $\delta^{13}C_{CH4}$ could be interpreted as thermogenic (Milkov and Etiope, 2018), noble gas data suggest that the CO_2 is magmatic in origin and the interpretation of gas origin in a magmatic – crustal gas system faces difficulties with this isotope pair (Snodgrass and Milkov, 2020).

4.2. Noble gases

$^3He/^4He$ ratios vary from 0.058 ± 0.004 (well #10) to 3.95 ± 0.11 R_A (well #12). With the exception of well #10, all samples exhibit a significant contribution of mantle derived He. Similar $^3He/^4He$ ratios has been reported from the Vaca Muerta by Brisson et al., (2020). Using the mean value of 8 R_A for the depleted upper mantle, the mantle contribution to the He varies from 24% (well #5) to 43% (well #12). If the He was derived from the sub-

TOTAL Classification: Restricted Distribution
TOTAL - All rights reserved

continental lithospheric mantle (SCLM) ($^3He/^4He$ of 6.84 R_A for southern Patagonia; Jalowitzki et al. (2016)) the mantle contribution varies from 28% to 58%.

The concentration of ^4He varies between 7.7 x 10^{-6} (field A, well #10) and 2.14 x 10^{-4} cm^3 STP/cm^3 (field A, well #6), though these are two outliers, with the majority of the samples exhibiting a narrow range between 2.40 and 9.09 x 10^{-5} cm^3 STP/cm^3. $^4He/^{20}Ne$ ratios from the twelve samples obtained from both fields and the Vaca Muerta and Mulichinco formations vary between 4,292 ± 248 (well #10) and 41,446 ± 2,348 (well #5). These are significantly above the air ratio of 0.32, showing that atmospheric contributions to all samples are negligible.

$CO_2/^3He$ ratios range from 6.27 x 10^9 (well #10) to 3.46 x 10^6 (well #5). The gases plot below the crustal and mantle range in $CO_2/^3He$-$\delta^{13}C_{CO2}$ space (Figure 4), implying the loss of CO_2 relative to He, as previously observed in numerous natural CO_2 accumulations (e.g. Gilfillan et al., 2009). Between 76% (well #6) to over 99% (well #5) of the CO_2 has been lost, assuming a mantle derived CO_2 end-member within the typical magmatic range of 1 to 10 x 10^9 (Marty and Jambon, 1987). Whilst the $CO_2/^3He$ of well #10 is within the MORB range, it is highly unlikely that the CO_2 contained in this sample is magmatic in origin, due to the crustal $^3He/^4He$ ratio (0.058 R_A) (crustal $^3He/^4He$ = 0.02 R_A, e.g. Ballentine, (1997)) and low CO_2 content. Hence, it is most likely that the CO_2 in this sample is the result of thermogenic production from the organic source rock.

The concentration of Ne for the sampled gases varies from 1.6 and 5.5 x 10^{-9} cm^3 STP/cm^3. Field A, well #10 exhibits both the lowest $^{20}Ne/^{22}Ne$ (9.89 ± 0.04) and $^{21}Ne/^{22}Ne$ (0.0310 ± 0.0004) values, which is consistent with the lowest observed $^3He/^4He$ ratio. Well #1 shows the highest $^{20}Ne/^{22}Ne$ (10.52 ± 0.05) and well #12 the highest $^{21}Ne/^{22}Ne$ (0.0455 ± 0.0004) values. There is no obvious difference in Ne isotope composition of Vaca Muerta and Mulichinco Formation gases. With the exception of well #10, all samples exhibit a significant contribution of mantle-derived Ne. The mantle Ne contribution ranges from 29% and 42% (Ballentine and O'Nions, 1991), similar to the contribution observed for He.

The concentration of Ar in the Vaca Muerta Shale gases from both fields varies between 2.6 x 10^{-6} (well #10) and 2.5 x 10^{-5} (well #7) cm^3 STP/cm^3. One of the Mulichinco Formation gases shows a similar concentration (1.35 x 10^{-5} in well #5) while the other is considerably higher (5.3 x 10^{-6} cm^3 STP/cm^3 in well #6). The $^{40}Ar/^{36}Ar$ ratios are significantly higher than the atmospheric value (298.6; Mark et al. (2011) and vary between 1,616 ± 18 (well #5) and

TOTAL Classification: Restricted Distribution
TOTAL - All rights reserved

3,674 ± 20 (well #7), indicative of excess of radiogenic, possibly mantle derived, ^{40}Ar. Elevated $^{40}Ar/^{36}Ar$ broadly correlate with increasing $^{3}He/^{4}He$. We observed no systematic differences between Vaca Muerta and Mulichinco Formations with respect to Ar isotopic compositions.

^{84}Kr and ^{132}Xe concentrations are distinct, both between fields A and B, and between the Vaca Muerta and Mulichinco Formations. ^{84}Kr concentrations from field A ($2.8 – 4.1 \times 10^{-10}$ cm^3 STP/cm^3) are lower than Mulichinco Formation (5.3×10^{-10} cm^3 STP/cm^3) and Vaca Muerta in field B (7.1×10^{-10} cm^3 STP/cm^3). ^{132}Xe exhibits similar increasing trends from between 3.9×10^{-11} cm^3 STP/cm^3 from field A, through 6.2×10^{-11} cm^3 STP/cm^3 from Mulichinco Formation to 9.9×10^{-11} cm^3 STP/cm^3 from field B. All noble gas data are summarised in Table 3.

5. Discussion

5.1. Relative timing of CO_2 injection into the Vaca Muerta Shale

Determining when the magmatic CO_2 was emplaced under the Vaca Muerta Formation is necessary in order to determine if there is a resolvable link between hydrocarbon generation in the shale (which occurred during the Late Cretaceous) (Brisson et al., 2020) and CO_2 emplacement. The earliest potential sources of magmatic CO_2 in the region is the Late Triassic-Early Jurassic rift volcanism (Spalletti et al., 2000). If CO_2 was generated during this event it was present during early maturation of hydrocarbons. Mantle melting in the late Cretaceous to Eocene related to basin uplift (Zamora Valcarce et al., 2009) could also be the source of the CO_2. Mantle melting events from early Miocene to intraplate volcanism in the early Pleistocene would have resulted in CO_2 emplacement under the shale (Gorring et al., 1997; Kay et al., 2004). A younger CO_2 source would result in an effective removal of hydrocarbons, and it would not be further diluted by new charging hydrocarbons.

The molecular composition of gas sampled for this study, compared to literature data obtained from the analysis of gases collected during drilling are plotted against the $\delta^{13}C_{CO2}$ values on Figure 3E. We observe an increasing dryness of the gas with increasingly heavy isotopic composition of the CO_2. Gases from field A show a strong positive correlation between CO_2 concentrations and gas dryness (Figure 3F). This suggests that the CO_2 in the Vaca Muerta Shale results in the displacement of the methane. However, significant desorption of the heavier hydrocarbons (C_2, C_3) is unlikely as the adsorption rate on Neuquén

TOTAL Classification: Restricted Distribution
TOTAL - All rights reserved

basin shales are similar to CO_2 (Zhao et al., 2017). This displacement process is likely to be the result of the adsorption of CO_2 and desorption of methane, effectively a natural analogue of CO_2-enhanced gas recovery technique for hydrocarbon production from shales (e.g. Iddphonce et al., 2020). This process can account for both a portion of the CO_2 loss observed in the $CO_2/^3He$ ratio measured on the produced gas (i.e. Figure 4, see Results section) and subsequent fractionation of $\delta^{13}C_{CO2}$. The absence of fractionation factors for CO_2 adsorption-desorption on shales, restricts us from determining the extent of CO_2 loss. The Mulichinco Formation data exhibits the same correlation between $\delta^{13}C_{CO2}$ and gas composition, suggesting either a different process of CO_2 loss or a different additional source of CO_2. In addition, the position of the Mulichinco data relative to the Vaca Muerta data (Figure 3E-F) suggests that hydrocarbon migration from the Vaca Muerta to the Mulichinco Formation alone is insufficient to explain the difference in the two datasets. In the absence of any observed correlation between CO_2 concentration and geothermal gradient we rule out significant heat-related hydrocarbon maturation with the presence of CO_2. Therefore, we reason that the correlation between the $\delta^{13}C_{CO2}$ and hydrocarbon composition strongly supports the notion that the CO_2 injection into the Vaca Muerta occurred after the maturation of the source rock.

5.2. Defining the origin and age of CO_2 within the Vaca Muerta Shale

The observation that CO_2 concentrations are highest where the two fault systems intersect (Figure 2) suggests that the majority of the CO_2 originates from below the Vaca Muerta Shale (see Section 2.1). Elevated concentrations of magmatic volatiles in gas samples from both fields confirms that the CO_2 originates from degassing mantle-derived magmatic bodies.

To determine the time of CO_2 emplacement into the crust beneath the Vaca Muerta Shale, we use He and Ne isotopes. Previous works demonstrated how $^3He/^4He$ ratio can be used to determine the fate of CO_2 if the initial composition of the gas components is known (Cranfield CO_2 enhanced oil recovery field; Györe et al., 2015; 2017). Significant CO_2 loss can be recognised when samples do not plot on the mixing curve in $^3He/^4He$-CO_2 space.

In this case, we can constrain the most likely end-member for the source of the CO_2 using the same methodology, assuming that the system is also a binary mix of mantle-derived magmatic CO_2 and hydrocarbons from the shales, as previously outlined in Section 4.2. and Figure 4. The magmatic CO_2 end-member has a $^3He/^4He$ between 3.95 R_A (highest measured, well #12) and 9 R_A (highest depleted upper mantle end-member) and a ^4He concentration

TOTAL Classification: Restricted Distribution
TOTAL - All rights reserved

which is above the highest measured (89.6 ppmv, well #7) but not above 200 ppmv, the upper limit of ^{4}He concentrations of magmatic CO_2 gases (Cornides et al., 1986; Marty et al., 1989; Zhou et al., 2012). The hydrocarbon component is best represented by gas from well #10 (0.4% CO_2, $^3He/^4He$ = 0.06 R_A, 7.7 ppmv ^{4}He) as discussed in section 4.2. This is typical of shale gases (Pujol et al., 2018) but has also been observed in coal-derived gases (Chen et al., 2019) obtained using similar unconventional gas extraction techniques. These end-members allow definition of (i) a mixing curve in the CO_2-$^3He/^4He$ space (Figure 5A) and (ii) a magmatic $CO_2/^3He$ value (Figure 5B). CO_2 loss from each sample can be calculated using both the CO_2-$^3He/^4He$ mixing curve (Györe et al., 2015) and by comparing $CO_2/^3He$ ratios to the calculated initial magmatic value of between 0.5 and 2.0 x 10^9. CO_2 dissolution in formation water is most likely to occur in permeable formations under the shale (see Section 2) (e.g. Gilfillan et al., 2009) and partly on the surface of the Vaca Muerta Shale by displacing mostly CH_4 (e.g. Liu et al., 2019). Using an inverse model, we calculate the CO_2 loss by the two methods for all Vaca Muerta samples (with the exception of the hydrocarbon gases of well #10), using the range of possible $CO_2/^3He$ and $^3He/^4He$ values for the end-member (see Appendix A1). Based on the *a priori* reasoning that the amount of CO_2 loss determined by each method should be in agreement when the fluid end-member compositions are correct, the end-members can be resolved. We calculate the optimum $^3He/^4He$, ^{4}He concentration and the initial $CO_2/^3He$ ratio within 1σ by minimising the difference between the CO_2 loss determined by the two methods. The optimum end-member values are $^3He/^4He_{magmatic}$ = 3.95-4.08 R_A, $^4He_{magmatic}$ = 111-200 ppmv, $^3He/^4He_{crust}$ = 0.007-0.03 R_A and $^4He_{crust}$ = 7.66-7.70 ppmv (see details in Appendix A1). The initial $CO_2/^3He$ is estimated to be between 8.8 and 16.0 x 10^8, which overlaps the mantle $CO_2/^3He$ range (Marty and Jambon, 1987). We note that CO_2 – $^3He/^4He$ data of Brisson et al., (2020) locate left from the mixing surface, which suggest that those also exhibit loss of CO_2, yet we are unable to quantify it in the absence of ^{4}He concentration data.

Assuming that the ^{4}He component contained in the magmatic CO_2 before its injection into the shallow crust originates from the mantle (e.g. Gilfillan and Ballentine, 2018), the post-injection ingrowth of radiogenic ^{4}He within the CO_2 allows the duration in the shallow crust to be estimated, assuming that the entire reservoir of ^{4}He produced had been released into the pore space. Using depleted mantle $^3He/^4He$ of 7-9 R_A and crustal compositions of ^{4}He and α particle producers (see Appendix A2) we determine that it takes between 11.8 and 35.6

TOTAL Classification: Restricted Distribution
TOTAL - All rights reserved

million years (mean 22.8 million years) to generate the $^{3}He/^{4}He$ end-member of 3.95-4.08 R_A (Figure 6A).

The Ne isotope composition of all samples plot within the air-crust-mantle region (Holland and Ballentine, 2006) (Figure 6B), allowing the Ne isotopic composition of the CO_2 end-member to be constrained. Gases from both fields define a straight line, trending towards the mantle - crust mix point. This trend is typical of a continuously degassing magmatic gas, which has not been trapped in the upper crust for a significant period of time, as demonstrated by recently charged magmatic gases contained within Bravo Dome (USA) (Baines and Worden, 2004; Ballentine et al., 2005; Gilfillan and Ballentine, 2018; Gilfillan et al., 2008). Bravo Dome is cited to have last experienced CO_2 injection between 1.2 and 1.5 million years ago (Sathaye et al., 2014) and exhibits a similar Ne isotopic trend to that of the Vaca Muerta data. The best-fit line of the data (n = 9) (excluding well #10 from field A) exhibits an $R^2 = 0.88$ consistent with mix between air-crust and mantle-crust end-members.

We can constrain the Ne isotopic composition of the crustal and mantle end-member by extrapolation of the mixing line to the mantle-crust and air-crust lines. We resolve the crustal $^{20}Ne/^{22}Ne$ of $9.77^{+0.02}_{-0.03}$, $^{21}Ne/^{22}Ne$ of $0.0313^{+0.0013}_{-0.0013}$ and the magmatic $^{20}Ne/^{22}Ne$ of $12.13^{+0.08}_{-0.10}$, $^{21}Ne/^{22}Ne$ of $0.074^{+0.004}_{-0.003}$. The crustal-air component contains 99.6% air-derived Ne. This is examined in more detail in Section 5.3. The magmatic composition is similar to the composition of the Patagonian SCLM determined by Jalowitzki et al. (2016) ($^{21}Ne/^{22}Ne$ = 0.065), which is only slightly below our lowest estimate within 1σ ($^{21}Ne/^{22}Ne$ = 0.071). In contrast, the intrinsic SCLM composition in their study exhibits a more nucleogenic composition ($^{21}Ne/^{22}Ne$ = 0.090). As nucleogenic ^{21}Ne accumulates over time in the crust, this suggests that the CO_2 present in the Vaca Muerta formation may originate from an aged depleted mantle-like source. Using the nucleogenic production rate of Ne isotopes (e.g. Ballentine and Burnard, 2002) we estimate the age of the CO_2 source. For a range of boundary conditions (see Appendix A2) we calculate the mean age range to be between 6 and 15 Ma, with the lowest and highest potential ages being 4.7 Ma and 20 Ma, within an error of 1σ. This is in a good agreement with the calculated mean He age of 22.8 Ma.

The He age represents a maximum age because the He closure temperature in the likely U- and Th-bearing mineral phases ranges from 60-180°C (e.g. Ault et al., 2019) while any additional source of ^{4}He from crustal flux (Sano et al., 1986; Torgersen et al., 1989) would lower the age. In contrast, Ne age likely represents a minimum age because there is no such

TOTAL Classification: Restricted Distribution
TOTAL - All rights reserved

crustal flux of Ne and the Ne closure temperature is significantly larger, ranging from 200-400°C from apatite to zircon (e.g. Gautheron et al., 2006), suggesting that a proportion of the Ne remained entrapped in the U/Th containing mineral. For geothermal gradient of ~40°C/km (Sylwan, 2014), the CO_2 reservoir would have to have been deeper than 1.5 and 5.0 km for the entire inventory of radiogenic He to be released. This generally seems to support the hypothesis on the CO_2 originating from at least 2.3 km deep (at least ~100°C), below the Auquilco Evaporite (see Figure 2).

The He and Ne in the magmatic CO_2 implies it was generated in the last 22.8 Myr. The likeliest source of the magmatic CO_2 is the melting associated with asthenosphere mantle upwelling induced by the collision of the Chile Trench and the South Chile Ridge around 14 Ma (Gorring et al., 1997; Jalowitzki et al., 2016). We suggest that a sub-salt CO_2 reservoir formed ~14 Ma and that CO_2 must have been injected into the Vaca Muerta Formation after this event. As the maturation of the source rock within the Vaca Muerta Formation is believed to have commenced in the Late Cretaceous, hydrocarbon must have been generated prior to the addition of CO_2 as indicated by the molecular composition – CO_2 concentration relationship (Section 5.1). Whilst additional thermal maturation after this event is possible, the absence of relationship between thermal anomalies and CO_2 concentrations tends to rule it out.

5.3. Unravelling mantle and air derived components in the gas samples

In order to constrain the origin of the fluids that have contributed to the noble gas fingerprint measured in the shale gases produced from the Vaca Muerta formation in both fields we use the measured air-derived noble gas and Ne isotopic ratios. We plot $^{20}Ne^{\dagger}/^{36}Ar$ (where $^{20}Ne^{\dagger}$ refers to the air derived ^{20}Ne) (Figure 7A), $^{84}Kr/^{36}Ar$ (Figure 7B) and $^{132}Xe/^{36}Ar$ (Figure 7C) against $^{20}Ne/^{22}Ne$. The binary mixing relationship between air and mantle-rich end-members displayed on the Ne three isotope plot is confirmed by the linear relationship by the majority of Vaca Muerta field A samples between $^{20}Ne/^{22}Ne$ and $^{20}Ne^{\dagger}/^{36}Ar$, $^{84}Kr/^{36}Ar$ and $^{132}Xe/^{36}Ar$. The exception are the two samples that exhibit the highest $^{20}Ne/^{22}Ne$ (wells #1, 12) which also show elevated $^{84}Kr/^{36}Ar$ and $^{132}Xe/^{36}Ar$. This linear mixing relationship allows both the air-derived and mantle-rich end-members of $^{20}Ne^{\dagger}/^{36}Ar$, $^{84}Kr/^{36}Ar$ and $^{132}Xe/^{36}Ar$ to be defined.

TOTAL Classification: Restricted Distribution
TOTAL - All rights reserved

In Section 5.2 we calculated that the $^{20}Ne/^{22}Ne$ air-derived end-member value contains 99.6% air-derived Ne (using the Ne 3-isotope plot air and crust end-member, Figure 6B), originating from the pore waters contained within the shale (as the elevated $^{4}He/^{20}Ne$ values rule out atmospheric contributions to the gases). Using the atmospheric $^{20}Ne/^{22}Ne$ end-member value of 9.81, we constrain the air derived composition for $^{20}Ne^{\dagger}/^{36}Ar$, $^{84}Kr/^{36}Ar$ and $^{132}Xe/^{36}Ar$, to be $0.426^{+0.056}_{-0.050}$, $0.099^{+0.013}_{-0.011}$ and $0.0152^{+0.023}_{-0.019}$, respectively. With respect to $^{20}Ne^{\dagger}/^{36}Ar$, this is between air (0.526) and air saturated water (ASW, 0.16) values, implying a ~4 times excess of air-derived Ne relative to the ASW end-member. Elevated Ne concentrations above 0.5 are not typically observed in groundwaters, the usual source cited for air-derived noble gases in the subsurface (Kipfer et al., 2002). However, previous studies (e.g. Podosek et al., 1980) have reported even greater Ne enrichments, particularly in kerogen rich shales (Torgersen et al., 2004). Similar enrichments in Ne have also been reported in hydrocarbon gases from New Mexico (Kennedy et al., 2002) and in Pakistan (Battani et al., 2000).

This atmospheric end-member also exhibits $^{84}Ke/^{36}Ar$ and $^{132}Xe/^{36}Ar$ ratios that are higher than air by factors of 4.7 (mean) and 20 (mean), respectively. High levels of Kr and Xe enrichment have also been reported in organic-rich shales (Torgersen et al., 2004), gases associated with conventional hydrocarbons (e.g. Kennedy et al., 2002) and unconventional gases obtained through the hydraulic fracturing process (Byrne et al., 2020). Hence, these elevated levels could be explained by enrichment on the source kerogen of the Vaca Muerta Shales, accessed through the natural 'injection' of CO_2 into Vaca Muerta, controlled by the critical temperature of the components ($T_{cKr}<T_{cXe}<T_{cCO2}$). As this gas component has no resolvable mantle volatile contribution (as shown by the low $^{3}He/^{4}He$ in well #10) we cite this composition to be the 'adsorbed gas' component retained within the source kerogen of the Vaca Muerta Shales, and term it *Component 1*.

The two samples that exhibit the highest $^{20}Ne/^{22}Ne$ values (wells #1, 12) show no evidence of mixing with this shale derived component. We suggest that this is the Ne isotopic composition of the deep sourced CO_2 that is generated somewhere under the shale prior to the release of *Component 1* into the gas phase. We resolve the $^{20}Ne/^{22}Ne$ of this to be 10.51 ± 0.04 (Appendix A3). Based on the mixing relationship between this mantle component, termed *Component 2*, and the adsorbed gas (*Component 1*), we calculate the composition of this end-member for $^{20}Ne^{\dagger}/^{36}Ar$, $^{84}Kr/^{36}Ar$ and $^{132}Xe/^{36}Ar$ to be $0.25^{+0.04}_{-0.06}$, $0.035^{+0.011}_{-0.016}$ and $0.0041^{+0.0019}_{-0.0028}$, respectively. For Ne, this is slightly above the ASW value of 0.16, though they overlap with ASW values for Kr and Xe, within one sigma error. Whilst this end-

TOTAL Classification: Restricted Distribution
TOTAL - All rights reserved

member exhibits elemental ratios that are similar to those of ASW, the possibility of undegassed water being present within the Vaca Muerta Shales when the magmatic CO_2 enters the formation is extremely unlikely.

Several studies have highlighted that the presence of a gas phase moving through groundwater can result in partial or complete 'stripping' of the ASW derived noble gases from the water into the gas phase (Barry et al., 2016; Darrah et al., 2014; Gilfillan et al., 2008; Györe et al., 2017; Pujol et al., 2018; Wen et al., 2016, Whyte et al., 2021). Based on this earlier works, we propose that the influx of magmatic derived CO_2 into the porous and permeable water filled sediments located below the Vaca Muerta Formation (e.g. Tordillo Formation, see Figure 1) will have resulted in the striping of ASW derived noble gases from the water into the magmatic CO_2. This is the likely origin of *Component 2*, as indicated by the elevated magmatic $^{20}Ne/^{22}Ne$ values and close to ASW elemental ratios.

Lastly, we resolve a third end-member, *Component 3*, through examination of the relationship between $^{20}Ne/^{22}Ne$ and noble gas elemental ratios within the field B data. As outlined in Section 5.2 and 5.3 (Figure 5 & 6) the magmatic CO_2 must be derived from a similar mantle source in both fields, however, as the migration pathway for the CO_2 to reach the Vaca Muerta Formation is different in the two fields, given that they are at different depths, the magmatic CO_2 will have interacted with a different volume of water in each case. This process generated *Component 2 and 3* with identical Ne isotopic composition but different composition with respect to the elemental ratios. If we therefore fit a mixing curve along field B data starting from *Component 1*, the elemental ratio composition of *Component 3* can be optimised for the best fit. We calculate the $^{20}Ne^{\dagger}/^{36}Ar$, $^{84}Kr/^{36}Ar$ and $^{132}Xe/^{36}Ar$ to be $0.066^{+0.063}_{-0.028}$, $0.0595^{+0.021}_{-0.024}$, and $0.0075^{+0.0040}_{-0.0041}$, respectively, which matches the $^{84}Kr/^{36}Ar$ and $^{132}Xe/^{36}Ar$ values measured in Vaca Muerta derived gases produced from wells #1 and 12 in field A (see Appendix A3).

5.4. Constraining the origin of the non-radiogenic noble gases

The clear mixing relationship between the air and mantle derived components observed in the Vaca Muerta derived shale gases in both fields within the Ne three isotope space indicates that the air and mantle end-members of each source are the same. Hence, the different ratios of the non-radiogenic noble gases observed in the mantle-volatile rich end-members (*Components 2 and 3*, Figure 7A-C) are most likely the result of a solubility related degassing

TOTAL Classification: Restricted Distribution
TOTAL - All rights reserved

processes which can be examined in more detail by focusing solely on the non-radiogenic noble gases.

Figure 8A depicts $^{84}Kr/^{36}Ar$ plotted against $^{20}Ne^{\dagger}/^{36}Ar$ and Figure 8B shows $^{132}Xe/^{36}Ar$ plotted against $^{20}Ne^{\dagger}/^{36}Ar$, along with the three resolved end-member components from section 5.3. The fractionation of ASW derived noble gas ratios within a gas phase that will result from the degassing of ASW in both a closed (via batch fractionation) and in an open system (via Rayleigh fractionation) is also shown (see e.g. Ballentine et al., 2002). Using this plot, we observe that the $^{20}Ne^{\dagger}/^{36}Ar$, $^{84}Kr/^{36}Ar$ and $^{132}Xe/^{36}Ar$ ratios within *Component 2* may be generated through the fractionation of ASW derived noble gases that would occur in both open and closed system degassing. As discussed in Section 5.3., the degassing of the groundwater present somewhere below the Vaca Muerta Shale can be expected to have occurred as a result of CO_2 migration, transferring ASW noble gases into the gas phase and then injected into the Vaca Muerta. Consequently, we know that it can be considered as an open system in terms of gas loss. With the notable exception of well #1, all Vaca Muerta field A data exhibit a binary mixing relationship between *Component 1* and *Component 2* within the envelopes constrained by the errors associated with each component. Hence, we suggest that the ASW noble gas signature within *Component 2* is generated through open system degassing close to the solubility controlled fractionation limit on the Rayleigh fractionation line, due to a relatively short contact between groundwater located below the Vaca Muerta Shale and the mantle derived CO_2. The signature observed in well #1 (Figure 8) suggests that the composition of ASW derived gases is more evolved and hence greater ASW degassing had occurred prior to mixing with the mantle derived CO_2.

Both of the Figure 8 plots highlight that the ratios observed in *Component 3* can only be generated through open system degassing of ASW into the gas phase, confirming that the system is open with respect to gas loss. The most probable explanation for *Component 3* is a longer contact of magmatic CO_2 – groundwater somewhere below Vaca Muerta, which may imply that the CO_2 – water contact is deeper than in case of *Component 2*. This is reflected in the Vaca Muerta field B data which exhibits a considerably more evolved ASW component. Using the constrained $^{20}Ne^{\dagger}/^{36}Ar$ uncertainty on *Component 3* we calculate this fractionation to have taken place until Gas/Water ratio has reached between 0.05 and 0.5, prior to the simply mixing with the mantle derived CO_2.

The $^{84}Kr/^{36}Ar$ and $^{132}Xe/^{36}Ar$ error of *Component 2 & 3* may be the result of the uncertainty of the mixing relationship defined in Section 5.3, but equally we are unable to rule out

TOTAL Classification: Restricted Distribution
TOTAL - All rights reserved

magmatic excess of Kr and Xe compared to ASW composition (along the fractionation line) and we calculate it to be ~1.5 and 4 times higher for Kr and Xe respectively. These Kr and Xe excesses are well within previous measurements from hydrocarbon gases (Ballentine et al., 2005; Holland and Ballentine, 2006), and below the level of excesses present in *Component 1*, the adsorbed source kerogen gases. Another possible explanation for the composition of *Component 3* would be the presence of oil in field B. However, elemental fractionation of $CO_2/^3He$ caused by the large differences in solubility of CO_2 and He (Ballentine et al., 2002) in oil would be inconsistent with the results of section 5.2 (Figure 5A-B) and therefore we reject this hypothesis.

The measured non-radiogenic noble gas signature of the field A Mulichinco samples can also be explained by a similar mixing between *Component 1* (source kerogen gas) and *Component 2*, with well #5 showing a slightly higher degree of ASW degassing. However, the significant depletion in Kr and Xe in well #6 implies that those components are difficult to transport from Vaca Muerta Shale into the overlying Mulichinco Formation, in line with previous observations of enrichments of heavy noble gases on kerogens.

5.5. CO_2 in the Mulichinco Formation

Field A Well #5, which contains gases produced conventionally from the Mulichinco Formation exhibits both the lowest CO_2 concentration of 0.08% and $CO_2/^3He$ ratio of 3.46×10^6, along with the lightest $\delta^{13}C_{CO2} = -12.8$ ‰. This suggests that there has been large amount of CO_2 loss relative to a magmatic source (see Figure 4). Adsorption of CO_2 on the Vaca Muerta Shales during transport through the entire Formation is a likely explanation for the additional CO_2 loss observed compared to the other samples and may also explain the significantly lighter $\delta^{13}C_{CO2}$ value (although fractionation factors are unknown for such systems). This is also corroborated by the observed Kr and Xe depletion (Figure 7B & C) in the Mulichinco Formation gases compared to those produced from the Vaca Muerta Formation. However, CO_2 loss into groundwaters within the Mulichinco Formation also remains a possibility.

In contrast, Field A well #6 exhibits both the highest measured CO_2 concentration of 24.2% and highest $CO_2/^3He = 2.35 \times 10^8$ (with the exception of well #10, as explained in section 5.1). This sample lies outside the envelope of the CO_2 loss model derived from combining the isotopic composition of the source CO_2 with He isotopic ratios (see Section 5.2). This means

TOTAL Classification: Restricted Distribution
TOTAL - All rights reserved

that we are unable to explain the composition of this sample through the addition of a single mantle derived source of CO_2 and subsequent CO_2 loss. However, we are able to show that this data would fit into the model if the CO_2 concentration was 70% lower (Figure 5A-B). As we also observe a more crustal-like Ne isotopic composition of both Mulichinco Formation samples (Figure 6B) compared to those sourced from the Vaca Muerta Formation, we suggest that non-magmatic CO_2 is present in the Mulichinco Formation.

A schematic summary of the processes that can account for the noble gas and stable isotopes of the gases from this study is provided in Figure 9. This work shows that integration of bulk gas composition, stable C isotopes and noble gas analysis are extremely useful in unravelling the origin of gas components and constraining their interactions in a complex hydrocarbon/water/magmatic system such as the Vaca Muerta Shale.

6. Conclusions

We present noble gas, molecular gas composition, $\delta^{13}C_{CH4}$, δD_{CH4} and $\delta^{13}C_{CO2}$ data for natural gases sampled from 12 wells in the Neuquén Basin. These samples were obtained from two producing fields, A and B, producing fluids from the unconventional source-rock reservoirs of the Vaca Muerta Formation and associated conventional hydrocarbons produced from the overlying Mulichinco Formation. We investigate the source, timing of emplacement and fate of the elevated CO_2 present in a number of samples using a combination of geochemical and isotopic composition of well gases along with structural geological observations from the study sites.

We observe elevated CO_2 concentrations when deep-rooted faults in the Auquilco Evaporite Formation, located below the Vaca Muerta Shale, overlap with shallower faults that grow from the top of evaporites into the shale, indicating a sub-evaporate origin of the CO_2. Increasing CO_2 concentrations are correlated with increasing $C_1/(C_2+C_3)$ values (4.8 – 33.5) and fractionation of $\delta^{13}C_{CO2}$ (-0.9 to -7.7 ‰), indicating the displacement of CH_4 by CO_2. This indicates that the CO_2 entered the shale after hydrocarbon maturation within the Vaca Muerta Formation had occurred.

The noble gas composition ($^3He/^4He$ of 3.43 – 3.95 R_A, $^{21}Ne/^{22}Ne$ of 0.0310 - 0.0455, $^{20}Ne/^{22}Ne$ of 9.89 - 10.52, $^{40}Ar/^{36}Ar$ of 2,432 – 3,674 and $CO_2/^3He$ 6.8 - 20.2 x 10^7) of the produced gases provides evidence that mixing between magmatic CO_2 and crustal hydrocarbon-rich gas sources has occurred in the subsurface. Using inverse modelling

TOTAL Classification: Restricted Distribution
TOTAL - All rights reserved

techniques and the relationship between $CO_2/^3He$ and $^3He/^4He$ we constrain the noble gas fingerprint of the original magmatic CO_2 prior to mixing with the hydrocarbons to be $^3He/^4He$ = 3.95 - 4.08 R_A, ^4He = 111-200 ppmv, $CO_2/^3He$ = 8.8-16.0 x 10^8, $^{20}Ne/^{22}Ne$ = 12.03-12.21 and $^{21}Ne/^{22}Ne$ = 0.071-0.078. Following magmatic degassing, this buoyant CO_2 then migrated up through permeable faults into the overlying Vaca Muerta and to the Mulichinco Formations.

Using the radiogenic ^4He and Ne we identify that their composition is consistent with radiogenic ingrowth within a depleted asthenosphere mantle-derived fluid, which has been trapped in the crust since 6.0 – 22.8 Ma. Melting as a result of mantle asthenospheric upwelling induced by the collision of the South Chile Ridge and the Chile Trench at ~14 Ma is the most likely source of this CO_2, significantly younger than the cited Late Cretaceous maturation of the hydrocarbon source rocks.

We further identify the presence of two distinct ASW-derived components derived from the water present below the shale on the basis of $^{20}Ne†/^{36}Ar$, $^{84}Kr/^{36}Ar$, $^{132}Xe/^{36}Ar$ ratios. These are consistent with early and late stage open system Rayleigh fractionation of ASW due to the CO_2 migrating buoyantly through the deep aquifer formations. We find evidence that both ASW-derived components premix with the magmatic CO_2, which then mixes with the previously adsorbed shale-derived gas. We conclude that the noble gas isotopes are capable of unravelling the origin and interaction history of fluids in a complex system such as the Vaca Muerta Shale.

Acknowledgements

The research was funded through the 'Isotope Coupling and Classical tools: Applications to Reservoir and Exploration (ICCARE)' project, sponsored by Total Exploration and Production (Total EP). Bernardo Collazo (Total EP Argentina) is thanked for dealing with customs and managing all logistics relating to sampling and their transport to the laboratories for analysis. Mariano Raverta (Total EP Argentina) is thanked to provide access to the field. Lorenzo Parigini (Total EP Argentina) is thanked for his help on the field, especially with the communication with the operators. Sebastian Estrada (Total EP Argentina) is thanked for discussions about the tectonics and structural geology of the area. Domonique Duclerc (Total EP) is thanked for her help resolving sampling issues in the field. Dr Marta Zurakowska and Dominique Duclerc are thanked for their help in the laboratories during analysis. Dr Ángel

TOTAL Classification: Restricted Distribution
TOTAL - All rights reserved

Rodés is thanked for help in the statistical methods applied to the data. Tom Darrah, Alexei Milkov and Donald Porcelli are thanked for their constructive review and editorial comments which helped to improve the manuscript.

Conflict of interest

The Authors declare no conflict of interest.

Author contribution

D.G., S.M.V.G., M.P., F.M.S.: Conceptualization of the project. M.P.: Sampling on the field. D.G.: Data acquisition. D.G., M.P., S.M.V.G.: Data interpretation with assistance of all co-authors. D.G.: First draft of the manuscript, calculations and coding. D.G., S.M.V.G., M.P., F.M.S.: Writing and editing.

TOTAL Classification: Restricted Distribution
TOTAL - All rights reserved

References

Ault, A.K., Gautheron, C. and King, G.E. (2019) Innovations in (U–Th)/He, Fission Track, and Trapped Charge Thermochronometry with Applications to Earthquakes, Weathering, Surface-Mantle Connections, and the Growth and Decay of Mountains. *Tectonics 38, 3705-3739, 10.2029/2018TC005312.*

Baines, S.J. and Worden, R.H. (2004) The long-term fate of CO_2 in the subsurface: natural analogues for CO_2 storage. *Geological Society, London, Special Publications 233, 59-85, 10.1144/GSL.SP.2004.233.01.06.*

Ballentine, C.J. (1997) Resolving the mantle He/Ne and crustal $^{21}Ne/^{22}Ne$ in well gases. *Earth. Planet. Sci. Lett. 152, 233-249, 10.1016/S0012-821X(97)00142-8.*

Ballentine, C.J., Burgess, R. and Marty, B. (2002) Tracing Fluid Origin, Transport and Interaction in the Crust, in: Porcelli, D., Ballentine, C.J., Wieler, R. (Eds.), Reviews in Mineralogy & Geochemistry Volume 47, Noble Gases in Geochemistry and Cosmochemistry, pp. 539-614, 10.2138/rmg.2002.47.13.

Ballentine, C.J. and Burnard, P.G. (2002) Production, Release and Transport of Noble Gases in the Continental Crust, in: Porcelli, D., Ballentine, C.J., Wieler, R. (Eds.), Reviews in Mineralogy & Geochemistry, 47, Noble Gases in Geochemistry and Cosmochemistry, pp. 481-538, 10.2138/rmg.2002.47.12.

Ballentine, C.J., Marty, B., Sherwood Lollar, B. and Cassidy, M. (2005) Neon isotopes constrain convection and volatile origin in the Earth's mantle. *Nature 433, 33-38, 10.1038/nature03182.*

Ballentine, C.J. and O'Nions, R.K. (1991) The nature of mantle neon contributions to Vienna Basin hydrocarbon reservoirs. *Earth. Planet. Sci. Lett. 113, 553-567, 10.1016/0012-821X(92)90131-E.*

Ballentine, C.J. and O'Nions, R.K. (1994) The use of natural He, Ne and Ar isotopes to study hydrocarbon-related fluid provenance, migration and mass balance in sedimentary basins. *Geol. Soc. Spec. Pub. 78, 347-361, 10.1144/GSL.SP.1994.078.01.23.*

Ballentine, C.J. and Sherwood Lollar, B. (2002) Regional groundwater focusing of nitrogen and noble gases into the Hugoton-Panhandle giant gas field, USA. *Geochim. Cosmochim. Acta 66, 2483-2497, 10.1016/S0016-7037(02)00850-5.*

Barry, P.H., Lawson, M., Meurer, W.P., Warr, O., Mabry, J.C., Byrne, D.J. and Ballentine, C.J. (2016) Noble gases solubility models of hydrocarbon charge mechanism in the Sleipner Vest gas field. *Geochim. Cosmochim. Acta 194, 291-309, 10.1016/j.gca.2016.08.021.*

Battani, A., Sarda, P. and Prinzhofer, A. (2000) Basin scale natural gas source, migration and trapping traced by noble gases and major elements: the Pakistan Indus basin. *Earth. Planet. Sci. Lett. 181, 229-249, 10.1016/S0012-821X(00)00188-6.*

Byrne, D.J., Barry, P.H., Lawson, M. and Ballentine, C.J. (2020) The use of noble gas isotopes to constrain subsurface fluid flow and hydrocarbon migration in the East Texas Basin. *Geochim. Cosmochim. Acta 268, 186-208, 10.1016/j.gca.2019.10.001.*

Brisson, I.E., Fasola, M.E. and Villar, H.J. (2020) Organic Geochemical Patterns of Vaca Muerta Shale, Neuquén Basin, Argentina. AAPG International Conference and Exhibition, Buenos Aires, Argentina, August 27-30, 10.1306/11302Brisson2020.

Chebli, G.A., Mendiberri, H., Giusiano, A., Ibañez, G. and Alonso, J. (2011) El shale gas en la Provincia del Neuquén, in: Stinco, L.P. (Ed.), Trabajos Técnicos: VIII Congreso de Exploración y Desarrollo de Hidrocarburos, 669-692 (in Spanish with English abstract).

TOTAL Classification: Restricted Distribution
TOTAL - All rights reserved

Chen, B., Stuart, F.M., Xu, S., Györe, D. and Liu, C. (2019) Evolution of coal-bed methane in Southeast Qinshui Basin, China: Insights from stable and noble gas isotopes. *Chem. Geol. 529, 10.1016/j.chemgeo.2019.119298.*

Coplen, T.B. (1994) Reporting of stable hydrogen, carbon, and oxygen isotopic abundances. *Pure Appl. Chem. 66, 273-276, 10.1351/pac199466020273.*

Cornides, I., Takaoka, N., Nagao, K. and Matsuo, S. (1986) Contribution of mantle-derived gases to subsurface gases in a tectonically quiescent area, the Carpathian Basin, Hungary revealed by noble gas measurements. *Geochem. J. 20, 119-125, 10.2343/geochemj.20.119.*

Craig, H. (1957) Isotopic standards for carbon and oxygen and correction factors for mass-spectrometric analysis of carbon dioxide. *Geochim. Cosmochim. Acta 12, 133-149, 10.1016/0016-7037(57)90024-8.*

Darrah, T.H., Jackson, R.B., Vengosh, A., Warner, N.R., Whyte, C.J., Walsh, T.B., Kondash, A.J. and Poreda, R.J. (2015) The evolution of Devonian hydrocarbon gases in shallow aquifers of the northern Appalachian Basin: Insights from integrating noble gas and hydrocarbon geochemistry. *Geochim. Cosmochim. Acta 170, 321-355, 10.1016/j.gca.2015.09.006.*

Darrah, T.H., Vengosh, A., Jackson, R.B., Warner, N.R. and Poreda, R.J. (2014) Noble gases identify the mechanism of fugitive gas contamination in drinking water wells overlying the Marcellus and Barnett Shales. *PNAS 111, 14076-14081, 10.1073/pnas.1322107111.*

Dominguez, R.F., Noguera, I.L., Continanzia, M.J., Mykietiuk, K., Ponce, C., Pérez, G., Guerello, R., Caneva, M., Di Benedetto, M., Catuneanu, O. and Cristallini, E. (2016) Organic-rich Stratigraphic Units in the Vaca Muerta Formation, and their Distribution and Characterization in the Neuquén Basin (Argentina). *Proceedings of the 4th Unconventional Resources Technology Conference, 1-3 August, San Antonio, Texas, USA, 10.15530/urtec-2016-2456851.*

Eberhardt, P., Eugster, O. and Marti, K. (1965) A redetermination of the isotopic composition of atmospheric neon. *Z. Naturforsch. 20a, 623-624, 10.1515/zna-1965-0420.*

Franzese, J.R. and Spalletti, L.A. (2001) Late Triassic - early Jurassic continental extension in southwestern Gondwana: tectonic segmentation and pre-break-up rifting. *JSAES 14, 257-270, 10.1016/S0895-9811(01)00029-3.*

Gangui, A. and Grausem, M. (2014) Estilos estructurales y tectonismo del intervalo Tithoniano-Valanginiano en el Engolfamiento Neuquino: implicancias en la interpretación de las fracturas monitoreadas por microsísmica en la Fm. Vaca Muerta. *IX Congreso de Exploración y Desarrollo de Hidrocarburos. p.: 341-364., Mendoza, Argentina, (in Spanish with English abstract).*

Gautheron, C.E., Tassan-Got, L. and Farley, K.A. (2006) (U–Th)/Ne chronometry. *Earth. Planet. Sci. Lett. 243, 520-535, 10.1016/j.epsl.2006.01.025.*

Gilfillan, S., Haszedline, S., Stuart, F., Györe, D., Kilgallon, R. and Wilkinson, M. (2014) The application of noble gases and carbon stable isotopes in tracing the fate, migration and storage of CO_2. *Energy Procedia 63, 4123-4133, 10.1016/j.egypro.2014.11.443.*

Gilfillan, S.M.V. and Ballentine, C.J. (2018) He, Ne and Ar 'snapshot' of the subcontinental lithospheric mantle from CO_2 well gases. *Chem. Geol. 480, 116-127, 10.1016/j.chemgeo.2017.09.028.*

Gilfillan, S.M.V., Ballentine, C.J., Holland, G., Blagburn, D., Sherwood Lollar, B., Scott, S., Schoell, M. and Cassidy, M. (2008) The noble gas geochemistry of natural CO_2 gas reservoirs from the Colorado Plateau and Rocky Mountain provinces, USA. *Geochim. Cosmochim. Acta 72, 1174-1198, 10.1016/j.gca.2007.10.009.*

TOTAL Classification: Restricted Distribution
TOTAL - All rights reserved

Gilfillan, S.M.V., Sherwood Lollar, B., Holland, G., Blagburn, D., Stevens, S., Schoell, M., Cassidy, M., Ding, Z., Zhou, Z., Lacrampe-Couloume, G. and Ballentine, C.J. (2009) Solubility trapping in formation water as dominant CO_2 sink in natural gas fields. *Nature 458, 614-618, 10.1038/nature07852.*

Gomes, I. and Brandt, R. (2016) Unconventional Gas in Argentina: Will it become a Game Changer? *The Oxford Institute of Energy Studies (OIES) Paper: NG 113, Oxford, UK, 10.26889/9781784670702.*

Gonfiantini, R. (1984) I.A.E.A. advisory group meeting on stable isotope reference samples for geochemical and hydrological investigations: Vienna, Austria, September 19–21, 1983. *Chem. Geol. 46, 85, 10.1016/0009-2541(84)90167-0.*

Gorring, M.L., Kay, S.M., Zeitler, P.K., Ramos, V.A., Rubiolo, D., Fernandez, M.I. and Panza, J.L. (1997) Neogene Patagonian plateau lavas: Continental magmas associated with ridge collision at the Chile Triple Junction. *Tectonics 16, 1-17, 10.1029/96tc03368.*

Györe, D. (2020) Ne component calculator. *MATLAB Central File Exchange.*, *https://www.mathworks.com/matlabcentral/fileexchange/74206-ne-component-calculator*.

Györe, D., Gilfillan, S.M.V. and Stuart, F.M. (2017) Tracking the interaction between injected CO_2 and reservoir fluids using noble gas isotopes in an analogue of large-scale carbon capture and storage. *Appl. Geochem. 78, 116-128, 10.1016/j.apgeochem.2016.12.012.*

Györe, D., McKavney, R., Gilfillan, S.M.V. and Stuart, F.M. (2018) Fingerprinting coal-derived gases from the UK. *Chem. Geol. 480, 75-85, 10.1016/j.chemgeo.2017.09.016.*

Györe, D., Stuart, F.M., Gilfillan, S.M.V. and Waldron, S. (2015) Tracing injected CO_2 in the Cranfield enhanced oil recovery field (MS, USA) using He, Ne and Ar isotopes. *Int. J. Greenh. Gas Con. 42, 554-561, 10.1016/j.ijggc.2015.09.009.*

Györe, D., Tait, A., Hamilton, D. and Stuart, F.M. (2019) The formation of NeH^+ in static vacuum mass spectrometers and re-determination of $^{21}Ne/^{20}Ne$ of air. *Geochim. Cosmochim. Acta 263, 1-12, 10.1016/j.gca.2019.07.059.*

Heilweil, V.M., Grieve, P.L., Hynek, S.A., Brantley, S.L., Solomon, D.K. and Risser, D.W. (2015) Stream measurements locate thermogenic methane fluxes in groundwater discharge in an area of shale-gas development. *Environ. Sci. Technol. 49, 4057-4065, 10.1021/es503882b.*

Hiyagon, H. and Kennedy, B.M. (1992) Noble gases in CH_4-rich gas fields, Alberta, Canada. *Geochim. Cosmochim. Acta 56, 1569-1589, 10.1016/0016-7037(92)90226-9.*

Hogg, S.L. (1993) Geology and hydrocarbon potential of the Neuquen Basin. *J. Pet. Geol. 16, 383-396, 10.1111/j.1747-5457.1993.tb00349.x.*

Holland, G. and Ballentine, C.J. (2006) Seawater subduction controls the heavy noble gas composition of the mantle. *Nature 441, 186-191, 10.1038/nature04761.*

Howell, J.A., Schwarz, E., Spalletti, L.A. and Veiga, G.D. (2005) The Neuquén Basin: an overview, in: Veiga, G.D., Spalletti, L.A., Howell, J.A., Schwarz, E. (Eds.), The Neuquén Basin: a Case Study in Sequence Stratigraphy and Basin Dynamics, The Geological Society London, Special Publication, 252, pp. 1-14, 10.1144/GSL.SP.2005.252.

Hunt, A.G., Darrah, T.H. and Poreda, R.J. (2012) Determining the source and genetic fingerprint of natural gases using noble gas geochemistry: A northern Appalachian Basin case study. *AAPG Bull 96, 1785–1811, 10.1306/03161211093.*

Iddphonce, R., Wang, J. and Zhao, L. (2020) Review of CO_2 injection techniques for enhanced shale gas recovery: Prospect and challenges. *J. Nat. Gas Sci. Eng. 77, 10.1016/j.jngse.2020.103240.*

TOTAL Classification: Restricted Distribution
TOTAL - All rights reserved

IEA (2019) Global Gas Security Review. *International Energy Agency, Paris,* *https://webstore.iea.org/download/direct/2832?fileName=Global_Gas_Security_Review_2019.pdf.*

Jalowitzki, T., Sumino, H., Conceição, R.V., Orihashi, Y., Nagao, K., Bertotto, G.W., Balbinot, E., Schilling, M.E. and Gervasoni, F. (2016) Noble gas composition of subcontinental lithospheric mantle: An extensively degassed reservoir beneath Southern Patagonia. *Earth. Planet. Sci. Lett. 450, 263-273, 10.1016/j.epsl.2016.06.034.*

Karolytė, R., Johnson, G., Györe, D., Serno, S., Flude, S., Stuart, F.M., Chivas, A.R., Boyce, A. and Gilfillan, S.M.V. (2019) Tracing the migration of mantle CO_2 in gas fields and mineral water springs in south-east Australia using noble gas and stable isotopes. *Geochim. Cosmochim. Acta 259, 109-128, 10.1016/j.gca.2019.06.002.*

Kay, S.M., Gorring, M. and Ramos, V. (2004) Magmatic sources, setting and causes of Eocene to Recent Patagonian plateau magmatism (36°S to 52°S latitude). *Asociación Geológica Argentina, Revista 59, 556-568.*

Kennedy, B.M., Torgersen, T. and van Soest, M.C. (2002) Multiple atmospheric noble gas components in hydrocarbon reservoirs: A study of the Northwest Shelf, Delaware Basin, SE New Mexico. *Geochim. Cosmochim. Acta 66, 2807-2822, 10.1016/S0016-7037(02)00883-9.*

Kipfer, R., Aeschbach-Hertig, W., Peeters, F. and Stute, M. (2002) Noble gases in lakes and ground waters, in: Porcelli, D., Ballentine, C.J., Wieler, R. (Eds.), Reviews in Mineralogy & Geochemistry, 47, Noble Gases in Geochemistry and Cosmochemistry, pp. 615-700, 10.2138/rmg.2002.47.14.

Langmuir, C.H., Vocke Jr, R.D., Hanson, G.N. and Hart, S.R. (1978) A general mixing equation with applications to Icelandic basalts. *Earth. Planet. Sci. Lett. 37, 380-392, 10.1016/0012-821X(78)90053-5.*

Legarreta, L., Laffitte, G.A. and Minnitti, S. (1999) Cuenca Neuquina: múltiplesposibilidades en las series jurásico–cretácicas del depocentro periandino, in: Chebli, G.A. (Ed.), Actas: IV Congreso Exploración y Desarrollo de Hidrocarburos, IAPG, Buenos Aires, pp. 145-147, (in Spanish).

Mamyrin, B.A., Anufrijev, G.S., Kamenskii, I.L. and Tolstikhin, I.N. (1970) Determination of the isotopic composition of atmospheric helium. *Geochem. Int.+ 7, 498-505*

Mark, D.F., Stuart, F.M. and de Podesta, M. (2011) New high-precision measurements of the isotopic composition of atmospheric argon. *Geochim. Cosmochim. Acta 75, 7494-7501, 10.1016/j.gca.2011.09.042.*

Marty, B. and Jambon, A. (1987) C / ^{3}He in volatile fluxes from the solid Earth: implications for carbon geodynamics. *Earth. Planet. Sci. Lett. 83, 16-26*

Marty, B., Jambon, A. and Sano, Y. (1989) Helium isotopes and CO_2 in volcanic gases of Japan. *Chem. Geol. 76, 25-40, 10.1016/0009-2541(89)90125-3.*

Matsuda, J., Matsumoto, T., Sumino, H., Nagao, K., Yamamoto, J., Miura, Y., Kaneoka, I., Takahata, N. and Sano, Y. (2002) The ^{3}He/^{4}He ratio of the new internal He Standard of Japan (HESJ). *Geochem. J. 36, 191-195, 10.2343/geochemj.36.191.*

Milkov, A.V., Faiz, M. and Etiope, G. (2020) Geochemistry of shale gases from around the world: Composition, origins, isotope reversals and rollovers, and implications for the exploration of shale plays. *Org. Geochem. 143, 10.1016/j.orggeochem.2020.103997.*

Milkov, A.V. and Etiope, G. (2018) Revised genetic diagrams for natural gases based on a global dataset of >20,000 samples. *Org. Geochem. 125, 109-120, 10.1016/j.orggeochem.2018.09.002.*

Mishima, K., Sumino, H., Otono, H., Yamada, T. and Oide, H. (2019) Accurate determination of the absolute ^{3}He/^{4}He ratio of a synthesized helium standard gas

TOTAL Classification: Restricted Distribution
TOTAL - All rights reserved

(Helium Standard of Japan, HESJ): toward revision of the atmospheric $^{3}He/^{4}He$ ratio. *Geochem. Geophys. Geosyst. 19, 3995-4005, 10.1029/2018GC007554.*

Moore, M.T., Vinson, D.S., Whyte, C.J., Eymold, W.K., Walsh, T.B. and Darrah, T.H. (2018) Differentiating between biogenic and thermogenic sources of natural gas in coalbed methane reservoirs from the Illinois Basin using noble gas and hydrocarbon geochemistry. *Geol. Soc. Spec. Pub., SP468.468, 10.1144/sp468.8.*

Nimz, G.J. and Hudson, G.B. (2005) The use of noble gas isotopes for monitoring leakage of geologically stored CO_2, in: Thomas, D.C., Benson, S.M. (Eds.), Carbon Dioxide Capture for Storage in Deep Geologic Formations, Elsevier, pp. 1113-1128

Ostera, H.A., García, R., Malizia, D., Kokot, P., Wainstein, L. and Ricciutti, M. (2016) Shale gas plays, Neuquén Basin, Argentina: chemostratigraphy and mud gas carbon isotopes insights. *Braz. J. Geol. 46, 181-196, 10.1590/2317-4889201620150001.*

Ozima, M. and Podosek, F.A. (2002) Noble Gas Geochemistry (2nd Ed.), Cambridge University Press, Cambridge, 367.

Pinti, D.L. and Marty, B. (1995) Noble gases in crude oils from the Paris Basin, France: Implications for the origin of fluids and constraints on oil-water-gas interactions. *Geochim. Cosmochim. Acta 59, 3389-3404, 10.1016/0016-7037(95)00213-J.*

Podosek, F.A., Honda, M. and Ozima, M. (1980) Sedimentary noble gases. *Geochim. Cosmochim. Acta 44, 1875-1884, 10.1016/0016-7037(80)90236-7.*

Prinzhofer, A., Monreal, F.R., Fasola, M. and Galliano, G. (2009) The Characterization of CO_2 Origins in the Neuquen Basin (Argentina): Mantle Fluids Influence for Oil Maturity and Gas Composition. *AAPG International Conference and Exhibition 15-18 November 2009, Rio de Janeiro, Brazil.*

Pujol, M., Van den Boorn, S., Bourdon, B., Brennwald, M. and Kipfer, R. (2018) Physical processes occurring in tight gas reservoirs from Western Canadian Sedimentary Basin: Noble gas signature. *Chem. Geol. 480, 128-138, 10.1016/j.chemgeo.2017.12.011.*

Rainoldi, A.L., Franchini, M., Beaufort, D., Patrier, P., Giusiano, A., Impiccini, A. and Pons, J. (2014) Large-Scale Bleaching of Red Beds Related To Upward Migration of Hydrocarbons: Los Chihuidos High, Neuquén Basin, Argentina. *J. Sediment. Res. 84, 373-393, 10.2110/jsr.2014.31.*

Ramos, V. (1981) Descripción geológica de la hoja 33c Los Chihuidos Norte, Provincia de Neuquén. *Servicio Geológico Nacional, Boletín 182, 1-103, (in Spanish).*

Sano, Y. and Marty, B. (1995) Origin of carbon in fumarolic gas from island arcs. *Chem. Geol. 119, 265-274, 10.1016/0009-2541(94)00097-R.*

Sano, Y., Wakita, H. and Huang, C.-W. (1986) Helium flux in a continental land area estimated from $^{3}He/^{4}He$ ratio in northern Taiwan. *Nature 323, 55-57, 10.1038/323055a0.*

Sathaye, K.J., Hesse, M.A., Cassidy, M. and Stockli, D.F. (2014) Constraints on the magnitude and rate of CO_2 dissolution at Bravo Dome natural gas field. *PNAS 111, 43, 15332-15337, 10.1073/pnas.1406076111.*

Schwarz, E., Spalletti, L.A., Veiga, G.D. and Fanning, C.M. (2016) First U–Pb SHRIMP age for the Pilmatué Member (Agrio Formation) of the Neuquén Basin, Argentina: Implications for the Hauterivian lower boundary. *Cretac. Res. 58, 223-233, 10.1016/j.cretres.2015.10.003.*

Sherwood Lollar, B., Ballentine, C.J. and O'Nions, R.K. (1997) The fate of mantle-derived carbon in a continental sedimentary basin: Integration of C/He relationships and stable isotope signatures. *Geochim. Cosmochim. Acta 61, 2295-2307, 10.1016/S0016-7037(97)00083-5.*

TOTAL Classification: Restricted Distribution
TOTAL - All rights reserved

Snodgrass, J.E. and Milkov, A.V. (2020) Web-based machine learning tool that determines the origin of natural gases. *Comput. Geosci. 145, 10.1016/j.cageo.2020.104595.*

Spacapan, J.B., Palma, J.O., Galland, O., Manceda, R., Rocha, E., D'Odorico, A. and Leanza, H.A. (2018) Thermal impact of igneous sill-complexes on organic-rich formations and implications for petroleum systems: A case study in the northern Neuquén Basin, Argentina. *Mar. Petrol. Geol. 91, 519-531, 10.1016/j.marpetgeo.2018.01.018.*

Spalletti, L.A., Franzese, J.R., Matheos, S.D. and Schwarz, E. (2000) Sequence stratigraphy of a tidally dominated carbonate–siliciclastic ramp; the Tithonian–Early Berriasian of the Southern Neuquén Basin, Argentina. *Journal of the Geological Society, London 157, 433-446, 10.1144/jgs.157.2.433.*

Stalker, L., Boreham, C., Underschultz, J., Freifeld, B., Perkins, E., Schacht, U. and Sharma, S. (2015) Application of tracers to measure, monitor and verify breakthrough of sequestered CO_2 at the CO2CRC Otway Project, Victoria, Australia. *Chem. Geol. 399, 2-19, 10.1016/j.chemgeo.2014.12.006.*

Staudacher, T., Sarda, P., Richardson, S.H., Allègre, C.J., Sagna, I. and Dmitriev, L.V. (1989) Noble gases in basalt glasses from a Mid-Atlantic Ridge topographic high at 14°N: geodynamic consequences. *Earth. Planet. Sci. Lett. 96, 119-133, 10.1016/0012-821X(89)90127-1.*

Sylwan, C. (2014) Source rock properties of Vaca Muerta Formation, Neuquina Basin, Argentina. *IX Congreso de Exploración y Desarrollo de Hidrocarburos Simposio de Recursos No Convencionales: Ampliando el Horizonte Energético.*

Torgersen, T. and Kennedy, B.M. (1999) Air-Xe enrichments in Elk Hills oil field gases: role of water in migration and storage. *Earth. Planet. Sci. Lett. 167, 239-253, 10.1016/S0012-821X(99)00021-7.*

Torgersen, T., Kennedy, B.M., Hiyagon, H., Chiou, K.Y., Reynolds, J.H. and Clarke, W.B. (1989) Argon accumulation and the crustal degassing flux of ^{40}Ar in the Great Artesian Basin, Australia. *Earth. Planet. Sci. Lett. 92, 43-56, 10.1016/0012-821X(89)90019-8.*

Torgersen, T., Kennedy, B.M. and van Soest, M.C. (2004) Diffusive separation of noble gases and noble gas abundance patterns in sedimentary rocks. *Earth. Planet. Sci. Lett. 226, 477-489, 10.1016/j.epsl.2004.07.030.*

Vergani, G.D., Tankard, A.J., Belotti, H.J. and Welsink, H.J. (1995) Tectonic evolution and paleogeography of the Neuquén Basin, in: Tankard, A.J., Suárez, S.R., Welsink, H.J. (Eds.), Petroleum Basins of South America, American Association of Petroleum Geologist, Memoir 62, pp. 383-402, 10.1306/M62593C19.

Wen, T., Castro, M.C., Ellis, B.R., Hall, C.M. and Lohmann, K.C. (2015) Assessing compositional variability and migration of natural gas in the Antrim Shale in the Michigan Basin using noble gas geochemistry. *Chem. Geol. 417, 356-370, 10.1016/j.chemgeo.2015.10.029.*

Wen, T., Castro, M.C., Nicot, J.P., Hall, C.M., Larson, T., Mickler, P. and Darvari, R. (2016) Methane Sources and Migration Mechanisms in Shallow Groundwaters in Parker and Hood Counties, Texas-A Heavy Noble Gas Analysis. *EnST 50, 12012-12021, 10.1021/acs.est.6b01494.*

Wen, T., Castro, M.C., Nicot, J.P., Hall, C.M., Pinti, D.L., Mickler, P., Darvari, R. and Larson, T. (2017) Characterizing the Noble Gas Isotopic Composition of the Barnett Shale and Strawn Group and Constraining the Source of Stray Gas in the Trinity Aquifer, North-Central Texas. *Environ. Sci. Technol. 51, 6533-6541, 10.1021/acs.est.6b06447.*

Whyte, C.J., Vengosh, A., Warner, N.R., Jackson, R.B., Muehlenbachs, K., Schwartz, F.W. and Darrah, T.H. (2021) Geochemical evidence for fugitive gas contamination and

TOTAL Classification: Restricted Distribution
TOTAL - All rights reserved

associated water quality changes in drinking-water wells from Parker County, Texas. *Sci. Total Environ. 780, 10.1016/j.scitotenv.2021.146555.*

Zamora Valcarce, G., Zapata, T., Ramos, V.A., Rodríguez, F. and Bernardo, L.M. (2009) Evolución tectónica del frente Andino en Neuquén. *Revista de la Geológica Argentina 65, 192-203, (in Spanish with English abstract).*

Zhao, H., Lai, Z. and Firoozabadi, A. (2017) Sorption Hysteresis of Light Hydrocarbons and Carbon Dioxide in Shale and Kerogen. *Sci Rep 7, 16209, 10.1038/s41598-017-13123-7.*

Zhou, Z., Ballentine, C.J., Kipfer, R., Schoell, M. and Thibodeaux, S. (2005) Noble gas tracing of groundwater/coalbed methane interaction in the San Juan Basin, USA. *Geochim. Cosmochim. Acta 69, 5413-5428, 10.1016/j.gca.2005.06.027.*

Zhou, Z., Ballentine, C.J., Schoell, M. and Stevens, S.H. (2012) Identifying and quantifying natural CO_2 sequestration processes over geological timescales: The Jackson Dome CO_2 Deposit, USA. *Geochim. Cosmochim. Acta 86, 257-275, 10.1016/j.gca.2012.02.028.*

TOTAL Classification: Restricted Distribution
TOTAL - All rights reserved

Figures

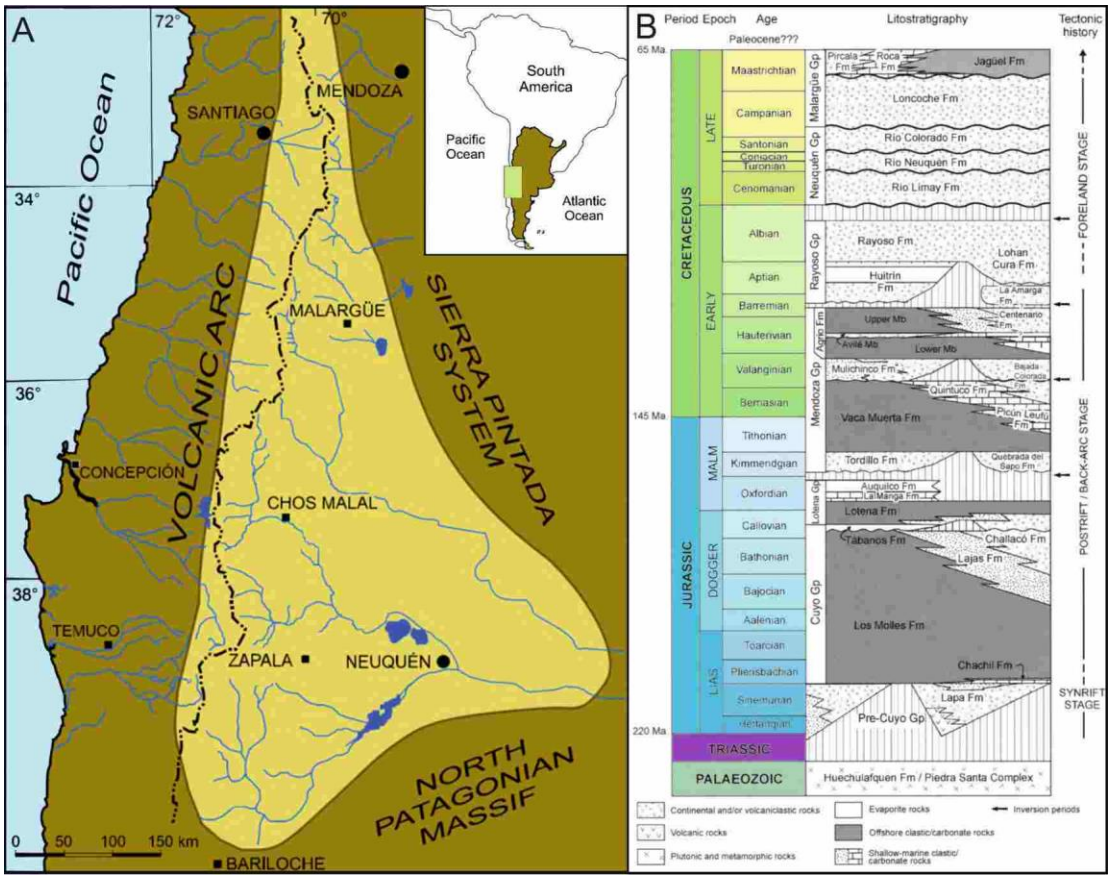

Figure 1. The location (A) and the stratigraphic column (B) of the Neuquén Basin. The study area is at the south part of the basin. Samples for this study are from the Vaca Muerta and Mulichinco Formations. Redrawn after Howell et al. (2005); Schwarz et al. (2016).

TOTAL Classification: Restricted Distribution
TOTAL - All rights reserved

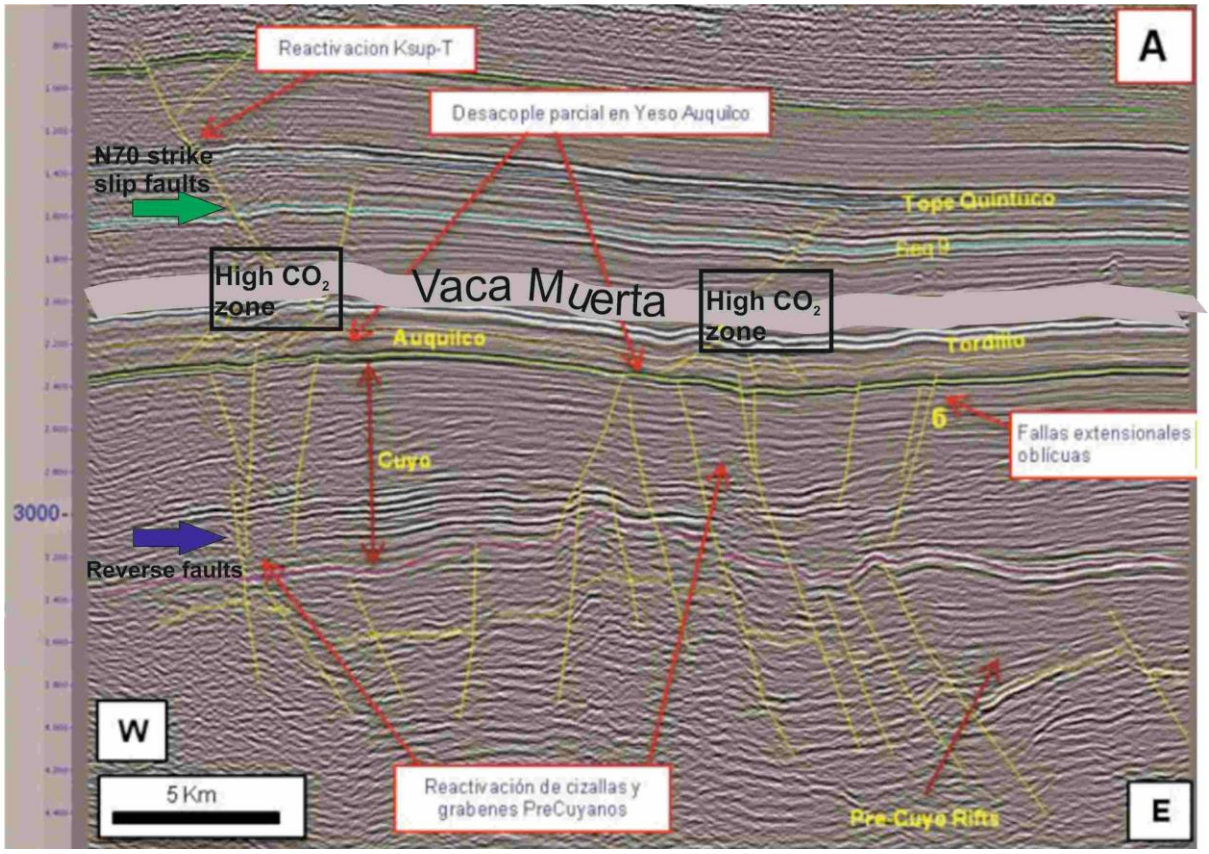

Figure 2. Seismic sections through field A showing fault control of CO_2 concentrations in the Vaca Muerta Formation. Two generations of faults are present. A deeply rooted, NNW trending series of, initially, normal faults that terminate in the Upper Jurassic Auquilco Evaporite Formation. They were reactivated as reverse faults in the early Cretaceous. N70 trending strike slip faults start in the Auquilco Formation and terminate in the Mulichinco Formation, cutting the Vaca Muerta Formation. The proportion of CO_2 in production wells increase drastically where the two fault systems intersect, suggesting that the CO_2 has a sub-salt origin. Redrawn after Gangui and Grausem (2014).

TOTAL Classification: Restricted Distribution
TOTAL - All rights reserved

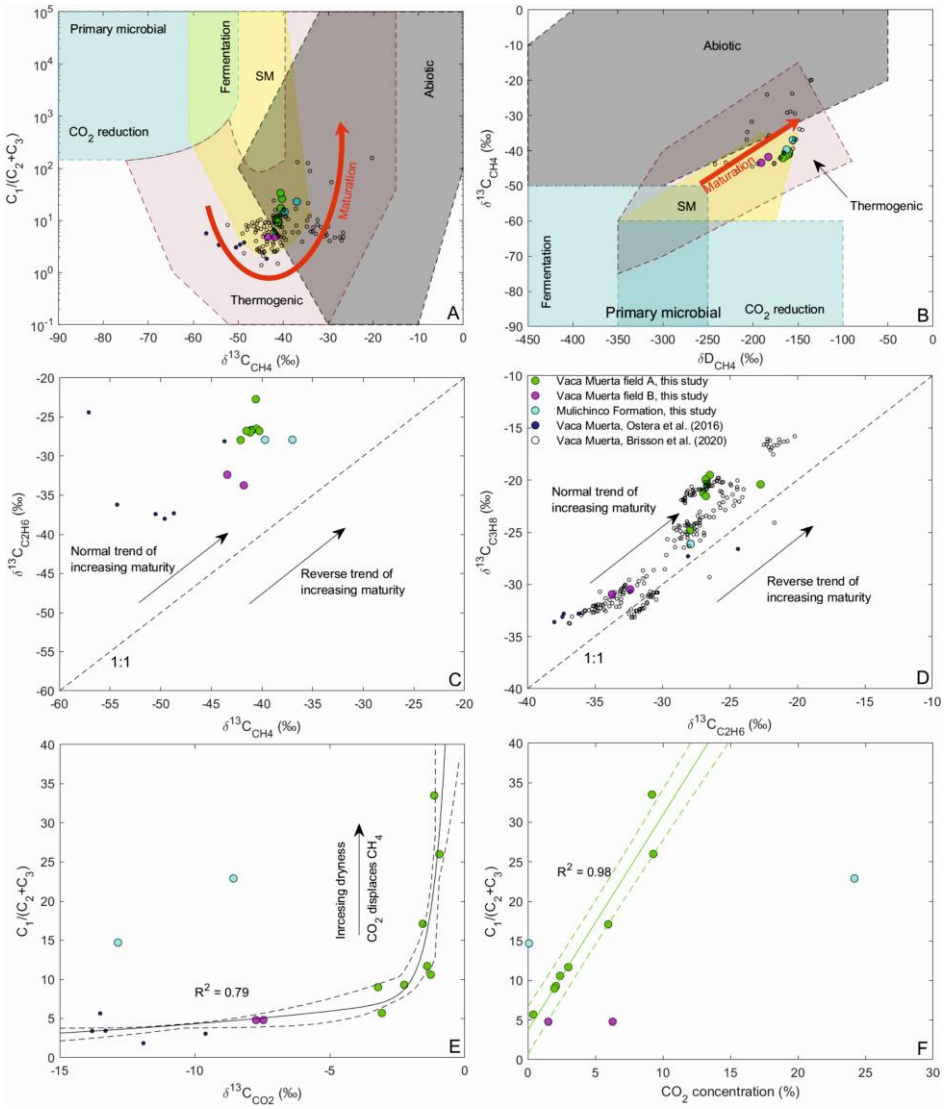

Figure 3. Molecular and stable isotopic composition of CO_2 and hydrocarbons for gases from the Vaca Muerta and Mulichinco Formations. $C_1/(C_2+C_3)$ vs. $\delta^{13}C_{CH4}$ (A) and $\delta^{13}C_{CH4}$ vs. δD_{CH4} (B) of well gases are consistent with gases of thermogenic origin. Our data show an increasingly mature gas compared to Vaca Muerta data from Ostera et al., (2016) and overlap with that of Brisson et al., (2020). Data from field B seem to be less mature than that of field A. SM: Secondary Microbial. (C, D): The isotopic composition of heavier hydrocarbons (C_2 – C_3) exhibit a normal trend of increasing maturity and confirms that field B data are less mature than field A data. Our data shows the same relationship to others' as above. Vaca Muerta data of this study combined with those of Ostera et al., (2016) exhibit a positive correlation with $\delta^{13}C_{CO2}$ (E). In field A, the same changes of the molecular composition also correlate with CO_2 concentration (F). We interpret this as methane desorption by natural CO_2 injection into the Vaca Muerta, an analogue for enhanced gas recovery similar to the process utilised to enhance gas recovery from coalbed methane fields (Zhou et al. 2005). Desorption of heavier hydrocarbons by CO_2 injection is unlikely due to their similar adsorption/desorption coefficients on shale than CO_2 (see text). This indicates that CO_2 injection into the shale occurred after source rock maturation. 1σ uncertainties are smaller than symbols. Redrawn after Milkov and Etiope, (2018) and Milkov et al., (2020). Data from Brisson et al., (2020) has been digitalized from their figures.

TOTAL Classification: Restricted Distribution
TOTAL - All rights reserved

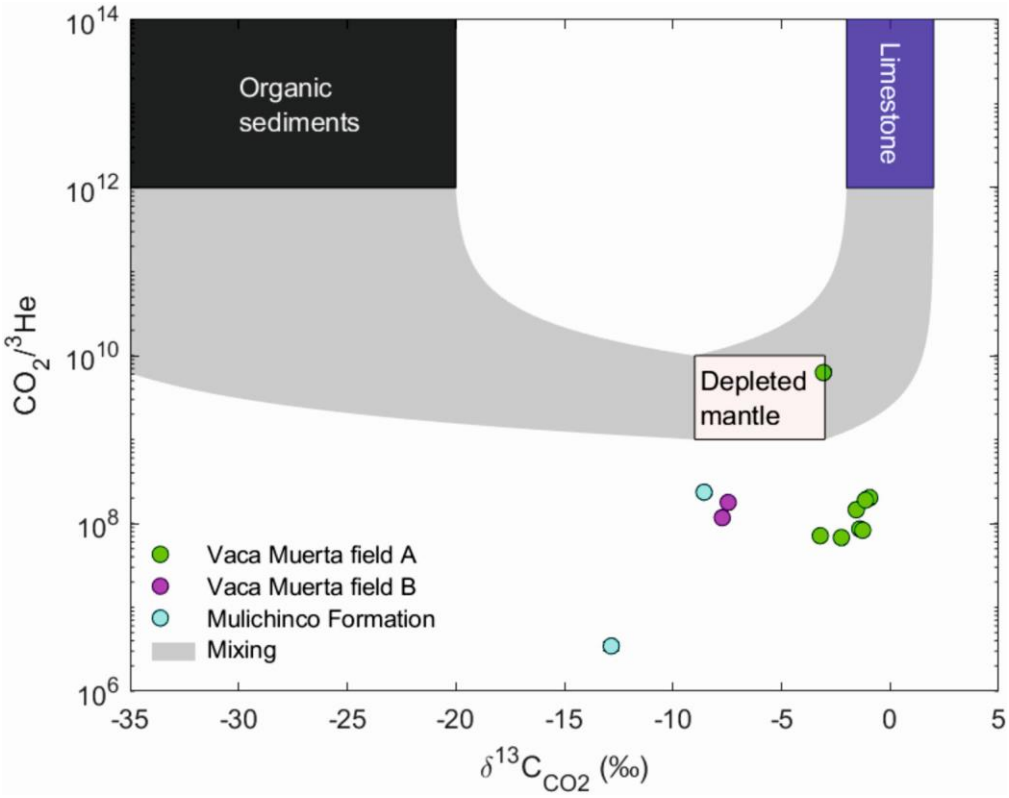

Figure 4. $CO_2/^3He$ against $\delta^{13}C_{CO2}$ for gases from the Vaca Muerta and Mulichinco Formations. Vaca Muerta (field A & B) except well #10 and Mulichinco Formation data plot below standard mixing fields. This is consistent with CO_2 loss relative to any source. Ranges of different sources are after Marty and Jambon (1987); Sano and Marty (1995). 1σ uncertainties are smaller than symbols.

TOTAL Classification: Restricted Distribution
TOTAL - All rights reserved

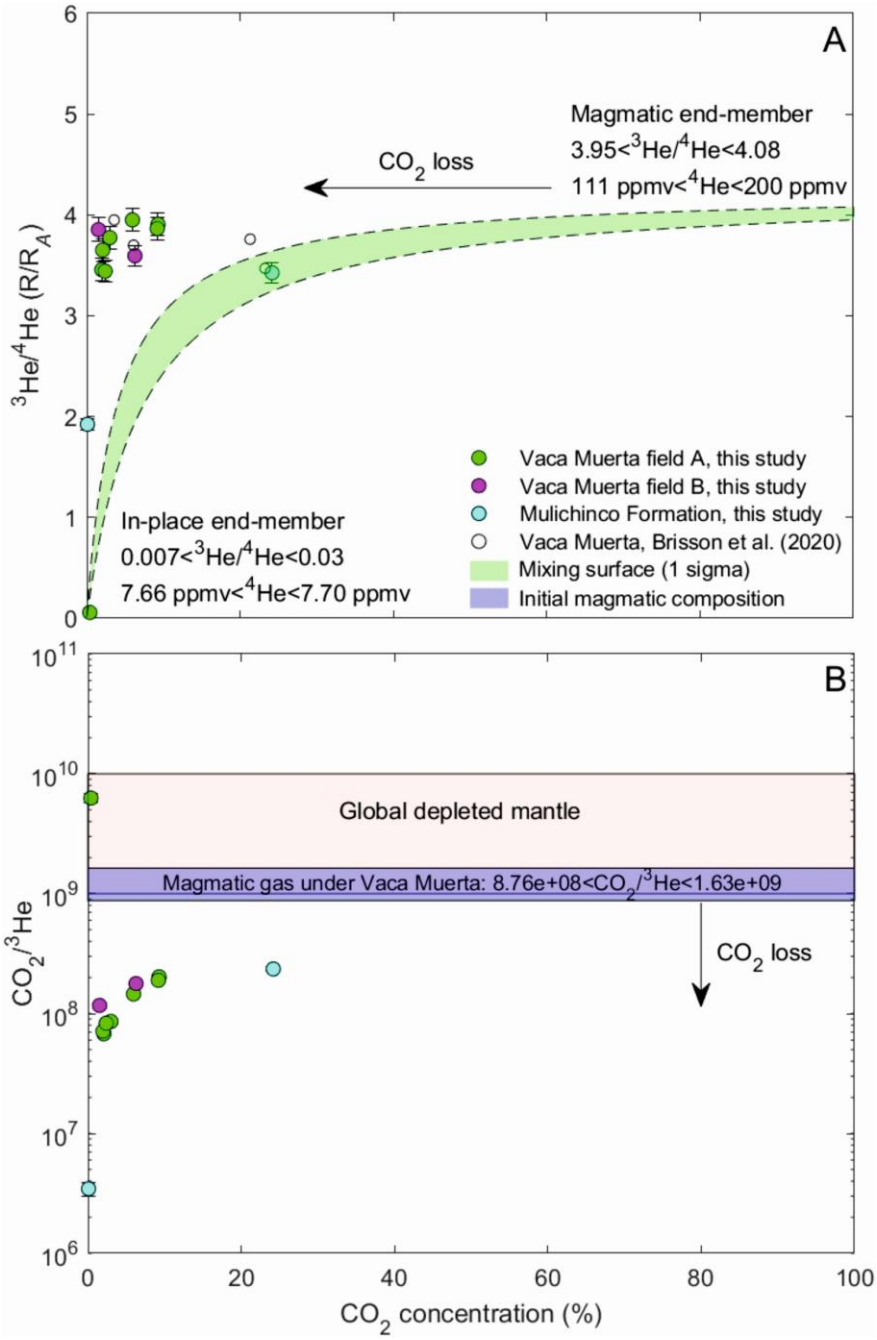

Figure 5. He-CO_2 systematics of well gases from the Neuquén Basin, Argentina. (A) Mixing between a crustal and magmatic gases for all Vaca Muerta samples apart from well #10 has been optimised within 1σ error (green surface). All data locate left from the surface, indicating a significant amount of CO_2 loss has occurred. The magmatic end-member defines the initial the $CO_2/^3He$ (B). The samples exhibit the same amount of CO_2 loss relative to the initial $CO_2/^3He$ (B), as relative to the mixing curve at their $^3He/^4He$ values (A). Well #6 from Mulichinco Formation does not fit into the model and suggests that ~70% of CO_2 originates from a different source to the common magmatic source in the other samples. Data from Brisson et al. (2020) suggest CO_2 loss too. MORB range is after Marty and Jambon (1987). Brisson et al., (2020) has been obtained via figure digitalization. Uncertainties are 1σ.

TOTAL Classification: Restricted Distribution
TOTAL - All rights reserved

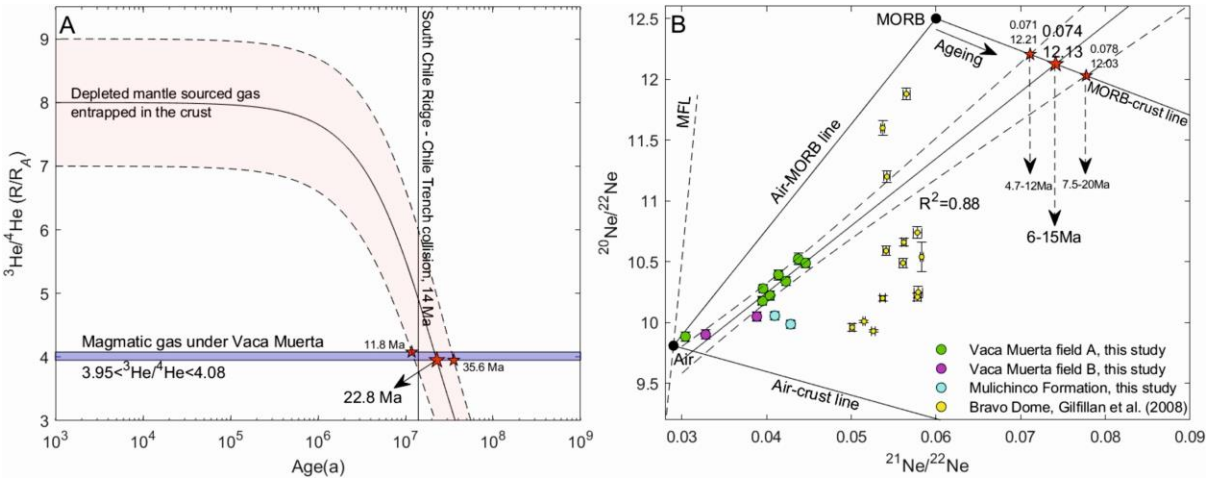

Figure 6. Constraints on the age of the CO_2 source in the Neuquén Basin. (A): Estimates on the mean age of the CO_2 (22.8 Ma) with no external source of ^{4}He. (B): The Vaca Muerta gases define a linear trend in Ne isotope space, consistent with a two-component mixing (see text). Extrapolating this trend to the upper mantle - crust mixing line yields a Ne isotope composition that overlaps the mantle composition recorded in Patagonia xenolits (Jalowitzki et al., 2016). We calculate the mean age of such depleted mantle derived gas trapped in the crust to be between 6.0-15 Ma. The collision of the South Chile Ridge and the Chile trench at ~14 Ma and subsequent astenospheric mantle upwelling is a possible source of melting and CO_2 release. Uncertainties are 1σ.

TOTAL Classification: Restricted Distribution
TOTAL - All rights reserved

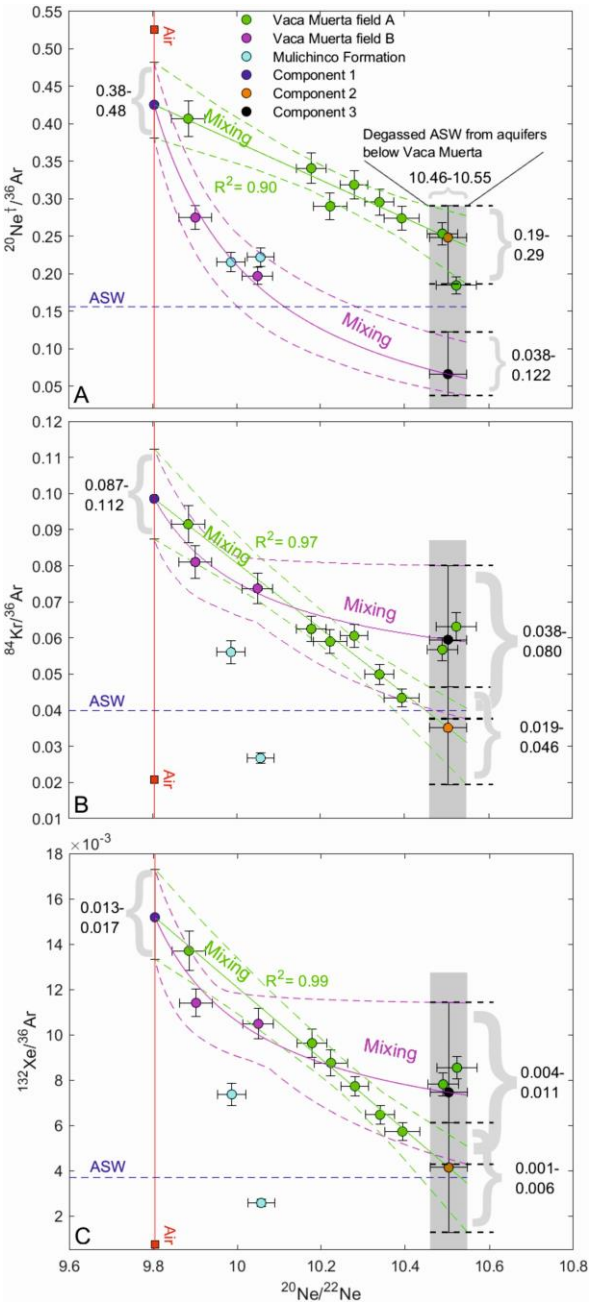

Figure 7. The plot of air-derived noble gas elemental ratios against $^{20}Ne/^{22}Ne$ for gas samples of the Neuquén Basin. Three distinct components are defined in the $^{20}Ne^{\dagger}/^{36}Ar$ (A), $^{84}Kr/^{36}Ar$ (B) and $^{132}Xe/^{36}Ar$ (C) space. 1): Air Ne isotopic composition (*Component 1*) is the adsorbed shale gas component. The two other components (*Component 2 & 3*) are magmatic for Ne isotopes (grey area), which are somewhere below Vaca Muerta and reached the shale prior to the release of *Component 1* and contain ASW derived gases. *Component 1* is released (desorbed) by the 'injection' of magmatic CO_2 - ASW mixture (*Component 2 & 3*). Linear mix (green) for Vaca Muerta field A data determines *Component 2*. Non-linear mix (purple) for Vaca Muerta field B data (best fit) determines *Component 3*. Mulichinco data are well explained by the purple mixing in the Ne-Ar space (A). Contrastingly, depletion of Kr and Xe is shown in the Mulichinco Formation relative to mixing, explained by their retention on the underlying Vaca Muerta Formation. Uncertainties are 1σ.

TOTAL Classification: Restricted Distribution
TOTAL - All rights reserved

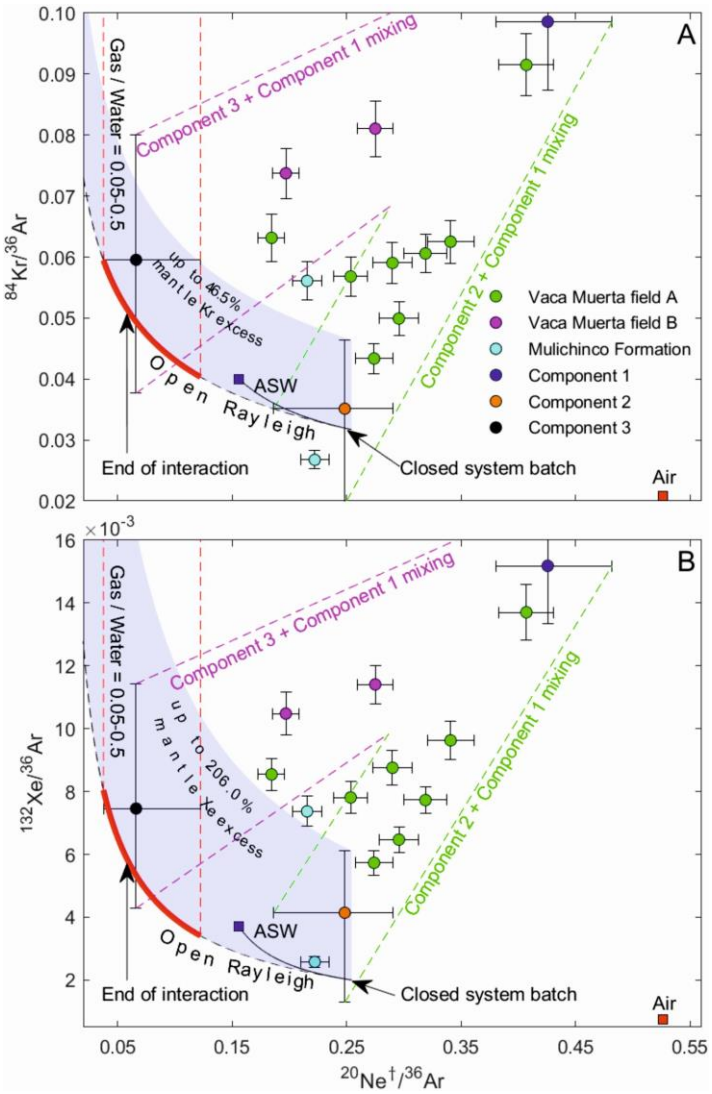

Figure 8. Plot of $^{84}Kr/^{36}Ar$ (A) and $^{132}Xe/^{36}Ar$ (B) against $^{20}Ne^{\dagger}/^{36}Ar$ for gas samples of the Neuquén Basin. Elemental ratios within *Component 2* and *3* are likely to be generated through the fractionation of ASW derived noble gases via interaction with CO_2 under Vaca Muerta, in an open system. *Component 2* is close to the solubility fractionation limit on the Rayleigh fractionation line due to a short interaction. *Component 3* is the result of an extensive degassing (G/W=0.06-0.4). These compositions once in the gas phase were present in the aquifer formations located under Vaca Muerta prior to its injection into the shale. These pre-mixed gases releases and mix with *Component 1* once injected into the shale. Vaca Muerta field A samples (except well #1) exhibit a binary mixing between *Component 1* and *2*. Well #1 composition suggests more evolved ASW derived gases, suggesting more interaction with formation waters. Vaca Muerta field B data exhibits a considerably more evolved ASW component and shows evidence of the mixing between *Component 3* and *1*. In *Component 2 & 3* we cannot rule out magmatic excess of Kr and Xe as an alternative of those components originating from formation waters. Well #5 of the Mulichinco Formation can also be explained by a similar mixing between early and later stage gases which have degassed ASW and *Component 1*. However, Kr and Xe depletion in well #6 implies that those components are difficult to desorb and transport from Vaca Muerta into the overlying Mulichinco Formation. Uncertainties are 1σ.

TOTAL Classification: Restricted Distribution
TOTAL - All rights reserved

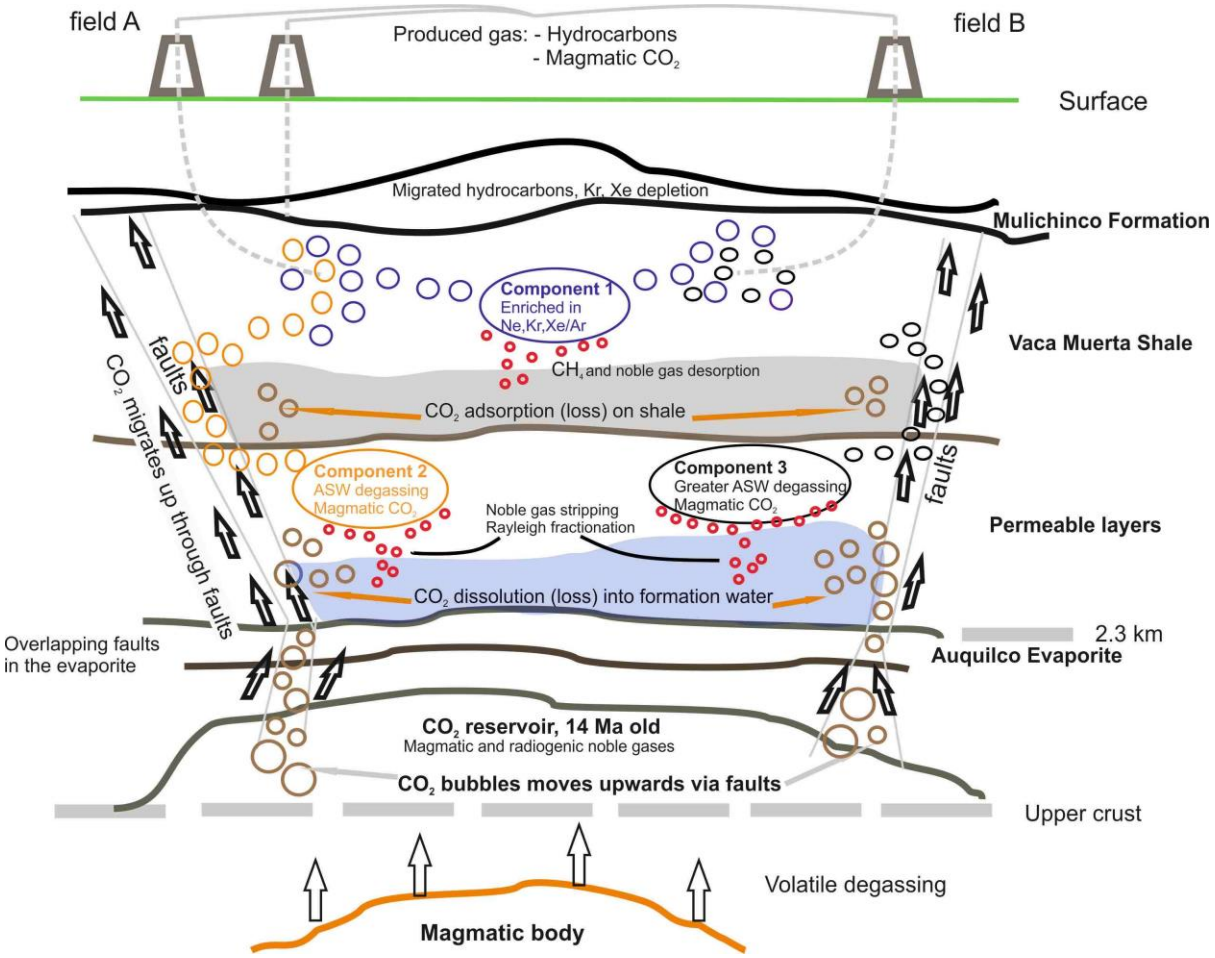

Figure 9. Synopsis of gas sources, evolution and mixing in the study fields of the Neuquén Basin. Magmatic CO_2 has been released into an upper crust reservoir under the Auquilco Evaporite Formation ~14 Ma ago. This CO_2 migrated up via permeable faults into the Vaca Muerta and Mulichinco Formations. During migration, a considerable amount of CO_2 has been lost into formation waters via dissolution within permeable layers under the Vaca Muerta. The process released air-derived noble gases from the formation water, controlled by the length (depth) of the CO_2 – water contact. Field A shows a short contact (*Component 2*), while field B experienced a longer contact (*Component 3*). When magmatic CO_2 along with these components entered the shale, it replaced methane, Kr and Xr in the shale (*Component 1*) and it also mixed with it. Depletion in Kr and Xe is observed within the samples from the Mulichinco Formation due to the difficulty in desorbing them from Vaca Muerta Shale.

TOTAL Classification: Restricted Distribution
TOTAL - All rights reserved

Tables

Table 1. Hydrocarbon and CO_2 concentrations from well gases of the Neuquén Basin.

Well	CH_4	C_2H_6	C_3H_8	CO_2	$C_1/(C_2+C_3)$	i-C_4H_{10}	n-C_4H_{10}	i-C_5H_{12}	n-C_5H_{12}
field A, Vaca Muerta									
#1	87.21	7.7	1.7	2.08	9.3	0.34	0.24	0.07	BDL
#2	88.38	6.4	1.2	3.00	11.7	0.22	0.15	0.04	0.02
#4	86.55	3.0	0.3	9.29	26.0	0.06	BDL	BDL	BDL
#7	87.35	2.4	0.2	9.19	33.5	0.03	0.02	BDL	BDL
#8	86.81	7.9	1.8	1.96	9.0	0.37	0.28	0.07	0.04
#9	87.68	6.8	1.5	2.39	10.6	0.30	0.23	0.07	0.03
#10	82.14	11.2	3.3	0.39	5.7	0.76	0.84	0.30	0.18
#12	87.96	4.5	0.6	5.95	17.1	0.13	0.08	0.02	0.01
field A, Mulichinco									
#5	91.81	4.8	1.4	0.08	0.08	0.29	0.39	0.15	0.10
#6	70.77	2.4	0.7	24.18	24.18	0.16	0.21	0.08	0.06
field B, Vaca Muerta									
#3	79.88	12.4	4.1	1.51	1.51	0.43	0.71	0.11	0.10
#11	75.37	10.6	5.0	6.28	6.28	0.51	0.84	0.11	0.11

Concentrations are mol/volume % under standard temperature and pressure (p = 0.101 MPa, T = 0 °C; Ozima and Podosek (2002)).
Relative uncertainties of concentrations are 1% (1σ). BDL: Below detection limit.

TOTAL Classification: Restricted Distribution
TOTAL - All rights reserved

Table 2. Stable isotopic compositions from well gases of the Neuquén Basin.

Well	$\delta^{13}C_{CO2}$	$\delta^{13}C_{CH4}$	δD_{CH4}	$\delta^{13}C_{C2H6}$	$\delta^{13}C_{C3H8}$	$\delta^{13}C_{i\text{-}C4H10}$	$\delta^{13}C_{n\text{-}C4H10}$
field A, Vaca Muerta							
#1	-2.2	-41.0	-160	-26.7	-20.4	-17.4	-16.7
#2	-1.4	-41.0	-161	-26.7	-20.0	-16.3	-15.9
#4	-0.9	-40.3	-160	-26.8	-19.9	-11.2	-15.4
#7	-1.1	-40.6	-164	-22.7	-20.4	-11.7	-17.5
#8	-3.2	-41.2	-161	-27.0	-21.2	-19.3	-16.7
#9	-1.3	-41.5	-164	-26.8	-21.5	-26.5	-18.4
#10	-3.1	-42.1	-166	-27.9	-24.8	-31.5	-22.9
#12	-1.6	-40.5	-160	-26.5	-19.5	-13.9	-15.3
field A, Mulichinco							
#5	-12.8	-39.7	-163	-27.9	-26.1	-25.0	-25.5
#6	-8.6	-37.0	-156	-27.9	-26.1	-27.2	-26.6
field B, Vaca Muerta							
#3	-7.7	-43.4	-191	-32.4	-30.5	-31.9	-29.3
#11	-7.5	-41.8	-183	-33.7	-30.9	-31.9	-29.3

Stable isotope data are in ‰. Carbon and hydrogen isotope data are relative to PDB and V-SMOW international standard respectively.
Absolute uncertainty of $\delta^{13}C$ is 0.12‰ and of δD is 1.0‰ (1σ).

TOTAL Classification: Restricted Distribution
TOTAL - All rights reserved

Table 3. Noble gas isotopic ratios and concentrations of well gases of the Neuquén Basin.

Well	$^{3}He/^{4}He$ (R/R_A)	$^{20}Ne/^{22}Ne$	$^{21}Ne/^{22}Ne$	$^{40}Ar/^{36}Ar$	^{4}He ($\times 10^{-5}$)	^{20}Ne ($\times 10^{-9}$)	^{40}Ar ($\times 10^{-5}$)	^{84}Kr ($\times 10^{-10}$)	^{132}Xe ($\times 10^{-11}$)	$^{20}Ne^{\dagger}$ ($\times 10^{-9}$)	$CO_2/^{3}He$ ($\times 10^{9}$)
field A, Vaca Muerta											
#1	3.65 (11)	10.52 (5)	0.0446 (4)	2432 (22)	5.99 (19)	1.62 (7)	1.35 (5)	3.51 (17)	4.75 (21)	1.03 (5)	0.68 (3)
#2	3.78 (11)	10.28 (3)	0.0405 (4)	2461 (17)	6.60 (25)	2.45 (10)	1.40 (5)	3.45 (14)	4.40 (17)	1.82 (8)	0.86 (4)
#4	3.91 (11)	10.39 (4)	0.0421 (5)	3060 (29)	8.40 (31)	2.74 (12)	2.11 (8)	2.99 (12)	3.96 (22)	1.89 (8)	0.20 (1)
#7	3.87 (11)	10.34 (4)	0.0431 (4)	3674 (20	8.96 (33)	2.86 (12)	2.50 (9)	3.40 (14)	4.40 (23)	2.01 (9)	0.19 (1)
#8	3.46 (11)	10.18 (4)	0.0403 (4)	2848 (25)	5.70 (21)	2.10 (9)	1.37 (5)	3.00 (12)	4.62 (24)	1.64 (7)	0.071 (4)
#9	3.44 (10)	10.22 (4)	0.0412 (4)	2788 (10)	5.97 (22)	2.02 (9)	1.46 (5)	3.11 (13)	4.61 (24)	1.53 (7)	0.083 (4)
#10	0.058 (4)	9.89 (4)	0.0310 (4)	626 (2)	0.77 (3)	1.79 (8)	0.26 (1)	3.85 (16)	5.77 (30)	1.71 (8)	6.27 (52)
#12	3.95 (11)	10.49 (4)	0.0456 (4)	3445 (17)	7.39 (28)	1.98 (8)	1.71 (6)	2.82 (12)	3.88 (20)	1.26 (6)	0.146 (7)
field A, Mulichinco											
#5	1.92 (6)	9.99 (3)	0.0437 (4)	1616 (18)	9.09 (34)	2.19 (9)	1.35 (5)	4.69 (19)	6.16 (32)	1.80 (8)	0.0035 (4)
#6	3.43 (10)	10.06 (3)	0.0417 (4)	2647 (10)	21.4 (8)	5.45 (23)	5.27 (20)	5.33 (22)	5.14 (27)	4.43 (19)	0.235 (11)
field B, Vaca Muerta											
#3	3.85 (12)	9.90 (4)	0.0334 (4)	976 (4)	2.40 (11)	2.57 (11)	0.85 (3)	7.05 (29)	9.93 (38)	2.39 (10)	0.117 (6)
#11	3.60 (10)	10.05 (4)	0.0396 (4)	1617 (9)	7.02 (26)	2.23 (9)	1.52 (6)	6.92 (29)	9.84 (52)	1.85 (8)	0.178 (8)
AIR	1.000 (9)	9.81 (8)	0.0290 (3)	298.6 (3)	0.52 (1)	16452 (36)	930 (1)	6498 (5)	2340 (3)	16452 (36)	0.056 (1)

Concentrations are in cm^3 (STP)/cm^3, standard temperature and pressure are p = 0.101 MPa, T = 0 °C after Ozima and Podosek (2002).
1σ uncertainties as last significant figures are in parenthesis.
$^{20}Ne^{\dagger}$ is the air-derived ^{20}Ne.
Air values are after Mamyrin et al. (1970) for He, Eberhardt et al. (1965) and Györe et al. (2019) for Ne, Mark et al. (2011) for Ar and Ozima and Podosek (2002) for Kr and Xe. We used 410 ppmv for atmospheric CO_2 concentration for $(CO_2/^{3}He)_{air}$.
Errors on $^{20}Ne^{\dagger}$ have been estimated by Monte Carlo simulation (n=20,000) (Györe, 2020).

TOTAL Classification: Restricted Distribution
TOTAL - All rights reserved

Appendix A

A1. Constraining the $^3He/^4He$ vs. CO_2 mixing curve

In order to resolve the most probable $CO_2/^3He$, $^3He/^4He$, $^4He_{crust}$ and $^4He_{magmatic}$ end-members the crustal and magmatic noble gas end-members were varied over the following ranges; $^3He/^4He_{magmatic}$ between 3.9 and 9 R_A, $^4He_{magmatic}$ concentration between 89.6 and 200 ppmv, $^3He/^4He_{crust}$ between 0.007 and 0.05 R_A and the $^4He_{crust}$ concentration between 7.5 and 7.7 ppmv (below $^4He_{crust}$ = 7.5 ppm the overall error increased). Each end-member variation defined a single mixing curve (Langmuir et al., 1978) and an initial $CO_2/^3He$ ratio.

CO_2 loss was calculated for each Vaca Muerta sample by 1) Calculating the theoretical CO_2 concentration at the measured $^3He/^4He$ value and the CO_2 loss by Eq. 1:

$$CO_{2\ loss\ 3He4He,i,n} = \frac{CO_{2\ theoretical,i,n} - CO_{2\ measured,i}}{CO_{2\ theoretical,i,n}} \quad \text{Eq.1}$$

And by 2) comparing measured $CO_2/^3He$ to that of determined by the end-member (initial) (Eq. 2.).

$$CO_{2\ loss\ CO23He,i,n} = \frac{CO_2/\ ^3He_{initial,n} - CO_2/\ ^3He_{measured,i}}{CO_2/\ ^3He_{initial,n}} \quad \text{Eq.2}$$

Where 'i' is the sample, 'n' is the location in the 4-dimension end-member matrix.

Because CO_2 loss for each sample must be equal given by Eq.1. and Eq.2., we calculated the differences for each sample ('i') at any given initial value ('n') (Eq.3):

$$CO_{2\ loss\ diff,i,n} = CO_{2\ loss\ 3He4He,i,n} - CO_{2\ loss\ CO23He,i} \quad \text{Eq.3}$$

and then we calculated the sum of the above difference for all samples (from i to m) at any given initial value 'n' by Eq.4.

$$CO_{2\ loss\ diff,total,n} = \sum_{m}^{i=1} \left| CO_{2\ loss\ 3He4He,i,n} - CO_{2\ loss\ CO23He,i,n} \right| \quad \text{Eq.4}$$

Where m is the number of samples.

We found best curves ±1 sigma where $CO_{2\ loss\ diff,total,n}$ is at minimum by χ^2 method. Minimum difference in the CO_2 loss at ideal end-members is given to be 5.2% (well #3) at the mean line. This is close the uncertainty on $CO_2/^3He$ measurements (4.9%, well #8).

A2. Calculation of He and Ne ages

For the He age calculation, we used the following average crustal concentrations: [U] = 2.8 ppmm, [Th] = 10.7 ppmm, [O] = 47.5%, [Mg] = 1.33%, [Na] = 2.89% (Ballentine and Burnard, 2002), a low O/F ratio of 112 (Kennedy et al., 1990) and $^3He/^4He_{mantle}$ = 7-9 R_A (Graham, 2002). We used the radiogenic ^4He production equation after Vermeesch, 2008 (Eq. 5) with a ^4He concentration of MORB ranging from 1.06 – 1.80 x 10^{-5} cm^3 (STP)/g (Graham et al., 1992).

$$^4He\left(\frac{mol}{g}\right) = \left(8\frac{137.88}{138.88}\left(e^{\lambda_{238}t}-1\right)+\frac{7}{138.88}\left(e^{\lambda_{235}t}-1\right)\right)x[U]+6\left(e^{\lambda_{232}t}-1\right)[Th] \qquad \text{Eq. 5}$$

Where $\lambda_{238,}$ $\lambda_{235,}$ λ_{232} are the decay constant of ^{238}U, ^{235}U and ^{232}Th and are 1.55 x 10^{-10}, 9.85 x 10^{-10} and 4.93 x 10^{-11}, respectively and 't' is time in years.

For the Ne age calculation, we used the crustal production rate equations from Ballentine and Burnard (2002) (Eq. 6-8).

$$^{20}\mathrm{Ne}(\mathrm{cm}^3(\mathrm{STP})/\mathrm{g/year}) = (6.39[\mathrm{U}]+0.77[\mathrm{Th}])(0.0226[\mathrm{O}]+0.0022[\mathrm{Na}])10^{-22} \qquad \text{Eq. 6}$$

$$^{21}\mathrm{Ne}(\mathrm{cm}^3(\mathrm{STP})/\mathrm{g/year}) = \{(1.48[\mathrm{U}]+0.186[\mathrm{Th}])[\mathrm{O}]+(0.105[\mathrm{U}]+0.0179[\mathrm{Th}])[\mathrm{Mg}]\}10^{-22} \qquad \text{Eq. 7}$$

$$^{22}\mathrm{Ne}(\mathrm{cm}^3(\mathrm{STP})/\mathrm{g/year}) = \{(3.06[\mathrm{U}]+0.417[\mathrm{Th}])[\mathrm{F}]+(4.2[\mathrm{U}]+0.663[\mathrm{Th}])[\mathrm{Mg}]\}10^{-24} \qquad \text{Eq. 8}$$

We used a $^3He/^{22}Ne$ ratio of between 8.3 – 9.8 (Jalowitzki et al., 2016; Staudacher et al., 1989). Using these ranges, we calculated the initial MORB ^{22}Ne = 1.06 – 2.76 x 10^{-11} cm^3 (STP)/g. We used end-member values of $^{21}Ne/^{22}Ne_{MORB}$ = 12.5 and $^{21}Ne/^{22}Ne_{MORB}$=0.06 (Ballentine et al., 2005; Holland and Ballentine, 2006).

A3. Constraint of the $^{20}Ne/^{22}Ne$, $^{20}Ne^{\dagger}$, ^{84}Kr, $^{132}Xe/^{36}Ar$ end-members

The Ne isotopic composition of the magmatic range was calculated using the best Gaussian fit to the probability density distribution of $^{20}Ne/^{22}Ne$ data of well #1 and 12 with 50,000

simulation steps. The linear fit to the majority of the Vaca Muerta field A data (except well #1 & 12) is calculated by Monte Carlo simulation (n=300,000) when both, 'x' and 'y' errors of the individual samples are considered and the one sigma error of the linear fit is provided. In the estimation of the elemental ratios of *Component 1*, the error on the air ($^{20}Ne/^{22}Ne$ = 9.81 ± 0.08) is not considered as it is the international standard and is not involved in the final error of the samples, as per standard practice.

The non-linear mean mixing curve in the Ne/Ar – NeNe space (Figure 7A) is determined as follows: Mixing curves are generated between the air mean end-member and reduced $^{20}Ne^{\dagger}/^{36}Ar$ values between that determined by the linear fit within the magmatic Ne end-member mean value and 0.008. Reduction in the $^{20}Ne^{\dagger}/^{36}Ar$ will also reduce $^{22}Ne/^{36}Ar$ relative to the initial value at the magmatic end. The initial value is calculated at 100% air, where $^{20}Ne = {}^{20}Ne^{\dagger}$ and is taken to be 0.043 (and remains constant along the linear mixing line). The best fit mixing curve along field B data by R^2 method defined the $^{20}Ne^{\dagger}/^{36}Ar$ and $^{22}Ne/^{36}Ar$ of the magmatic end-member. Using the determined $^{22}Ne/^{36}Ar$ at Ne magmatic mean value ($0.0115^{+0}_{-0.0078}$) we found resolved the best-fit mixing curve in the Kr/Ar and Xe/Ar spaces by the same method. For 1 sigma error estimation we repeated the experiment by replacing field B data with simulated data within the 1 sigma errors of the measured data, *Component 1*, magmatic Ne end-member and magmatic slope values (n = 300,000). All calculations and simulations have been coded in Matlab.